BOREAL ENVIRONMENT RESEARCH 27: 1–31
ISSN 1797-2469 (online)

Helsinki 21 March 2022

25 years of atmospheric and ecosystem measurements in a boreal forest — Seasonal variation and responses to warm and dry years

Ivo Neefjes[1)*], Mikko Laapas[2)], Yang Liu[3)], Erika Médus[2)], Elina Miettunen[4)], Lauri Ahonen[1)5)], Lauriane Quéléver[1)], Juho Aalto[1)5)], Jaana Bäck[6)], Veli-Matti Kerminen[1)], Janne Lampilahti[1)], Krista Luoma[1)], Mari Mäki[6)], Ivan Mammarella[1)], Tuukka Petäjä[1)], Meri Räty[1)], Nina Sarnela[1)], Ilona Ylivinkka[1)5)], Simo Hakala[1)], Markku Kulmala[1)], Tuomo Nieminen[1)] and Anna Lintunen[1)6)]

[1)] *Institute for Atmospheric and Earth System Research/Physics, Faculty of Science, University of Helsinki, P.O. Box 64, 00014 Helsinki, Finland (*corresponding author's e-mail: ivo.neefjes@helsinki.fi)*
[2)] *Finnish Meteorological Institute, P.O. Box 503, 00101 Helsinki, Finland*
[3)] *Department of Geosciences and Geography, University of Helsinki, P.O. Box 64, 00014 Helsinki, Finland*
[4)] *Finnish Environment Institute, Latokartanonkaari 11, 00790 Helsinki, Finland*
[5)] *Station for Measuring Ecosystem — Atmosphere Relations II (SMEAR II), University of Helsinki, 35500 Korkeakoski, Finland*
[6)] *Institute for Atmospheric and Earth System Research/Forest Sciences, Faculty of Agriculture and Forestry, University of Helsinki, P.O. Box 27, 00014 Helsinki, Finland*

Received 4 Jul. 2021, final version received 26 Jan. 2022, accepted 11 Feb. 2022

Neefjes I., Laapas M., Liu Y., Médus E., Miettunen E., Ahonen L., Quéléver L., Aalto J., Bäck J., Kerminen V-M., Lamplahti J., Luoma K., Mäki M., Mammarella I., Petäjä T., Räty M., Sarnela N., Ylivinkka I., Hakala S., Kulmala M., Nieminen T. & Lintunen A. 2022: 25 years of atmospheric and ecosystem measurements in a boreal forest — Seasonal variation and responses to warm and dry years. *Boreal Env. Res.* 27: 1–31.

Boreal forests are an important source of trace gases and atmospheric aerosols, as well as a crucial carbon sink. As such, they form a strongly interconnected coupled system with the atmosphere. The SMEAR II station is located in a boreal Scots pine forest in Hyytiälä, Finland, and has over 25 years of continuous measurements of atmospheric and ecosystem variables. In this study, we analyse the seasonal variations of trace gases, atmospheric aerosols, greenhouse gases, and meteorological variables, measured at the SMEAR II station during the past two and a half decades. Several ecosystem and atmospheric variables show seasonal correlations with each other, which suggests seasonal interactions within the climate system that links together ecosystem processes, greenhouse gases, trace gases and atmospheric aerosols. For instance, increased global radiation in summer increases air temperature and consequently affects the plant phenology, which promotes the ecosystem carbon exchange and biogenic volatile organic compound (biogenic VOC) release. This further affects the ambient concentrations of highly oxygenated organic molecules (HOMs) as well as the formation and growth of atmospheric organic aerosols. Organic aerosols subsequently influence aerosol optical properties and, through increased scattering, have

Editor in charge of this article: Albert Porcar-Castell

the potential to cool the climate. We also discuss the impacts of the warm and dry summers of 2010 and 2018 on the studied variables. For these years, we find a higher-than-average ecosystem primary production especially in June, leading to an increased VOC flux from the forest. The increased VOC flux in turn leads to higher HOM and secondary aerosol concentration in the atmosphere. The latter increases light scattering by atmospheric aerosol particles and thus leads to climate cooling. The results obtained in this study improve our understanding of how boreal forests respond to climate change.

Introduction

Boreal forests make up 27% of the world's forest landscape (FAO, 2020) and are an important source of trace gases and aerosols, releasing about 10% of the global biogenic volatile organic compound (BVOC) budget (Guenther 2013), and contributing 12–50% of the local atmospheric aerosol mass over Fennoscandia (Tunved *et al.* 2008). Furthermore, the boreal forest plant biomass is an important carbon sink, constituting > 25% of the global terrestrial carbon sink (Tagesson *et al.* 2020).

Terrestrial ecosystems, such as boreal forests, form a strongly interconnected coupled system with the atmosphere. The boreal ecosystem continuously fixes atmospheric carbon and emits carbon to the atmosphere through photosynthesis and respiration, respectively, and emits BVOCs during, e.g., plant growth and reproduction, and organic matter decomposition (e.g., Hakola *et al.* 2017, Mäki *et al.* 2019). Biogenic and anthropogenic volatile organic compounds (VOCs) are highly susceptible to oxidation reactions involving hydroxyl and nitrate radicals as well as ozone in the atmosphere (Schulze *et al.* 2017). Monoterpenes emitted by the forest ecosystem, for instance, produce highly oxygenated organic molecules (HOMs) in the atmosphere (Ehn *et al.* 2014, Bianchi *et al.* 2019). HOMs can in turn contribute to the formation of atmospheric aerosol particles by clustering with other gas-phase molecules, or by condensing onto a pre-existing atmospheric aerosol particle population (Mutzel *et al.* 2015, Bianchi *et al.* 2019).

The formation of atmospheric aerosol particles through the clustering of gas-phase molecules is called new particle formation (NPF). NPF is the main source of the total aerosol particle number concentration in the global atmosphere (Yu and Luo 2009, Gordon *et al.* 2017). The full range of gas-phase molecules that play a part in NPF is currently unknown. In continental regions, sulfuric acid has been established as a crucial component in NPF (Sipilä *et al.* 2010). HOMs were also found to contribute to NPF and are able to explain the majority of the observed particle growth from 2 nm up to 50 nm in boreal forests (Ehn *et al.* 2014). Aerosols that are mainly formed by condensation of oxidation products of organic molecules, such as HOMs, are also called secondary organic aerosols (SOA). Atmospheric aerosol particles have a net cooling effect on the global climate both directly, by scattering solar radiation (Kurtén *et al.* 2003, Lihavainen *et al.* 2009), and indirectly, by functioning as cloud condensation nuclei (CNN; Wiedensohler *et al.* 2009, Paramonov *et al.* 2013). They can also cause health problems by inhalation into the lungs. When studying air quality and the effect of atmospheric aerosol particles on the climate, both the number of atmospheric aerosol particles, as well as their mass and their composition, are important quantities.

BVOC emissions from the boreal forest ecosystems thus have a potential to influence the climate through oxidation into HOMs and subsequent atmospheric aerosol particle formation (e.g., Spracklen *et al.* 2008, Lihavainen *et al.* 2015, Kulmala *et al.* 2020, Petäjä *et al.* 2021). To elucidate these complex interactions more precisely between meteorological conditions (e.g., radiation, precipitation, and wind speed), ecosystem processes (e.g., carbon fixation and emission, and BVOC emission), and atmospheric variables (e.g., trace gas and atmospheric aerosol particle concentration), it is instructive to study seasonality. Correlations in seasonal patterns can indicate underlying

interrelated mechanisms between variables. Boreal forest ecosystems are highly affected by seasonality (e.g., Rantala *et al.* 2015, Dada *et al.* 2017, Nadal *et al.* 2021). Variations in for instance radiation or temperature highly impact the photosynthetic response of plants and consequent atmospheric aerosol particle formation originating from plant emissions. Atmospheric processes, such as HOM formation, are, furthermore, directly affected by radiation and temperature (Kontkanen *et al.* 2016, Bianchi *et al.* 2019, Quéléver *et al.* 2019). It is, therefore, crucial to study seasonal variations in the ecosystem and atmosphere and how these changes interrelate.

Global warming is more pronounced in the boreal and arctic region than elsewhere, with temperatures increasing twice as fast as the global average (IPCC, 2021). The forest's response to climate change is, however, still poorly understood. Climate warming is expected to result in longer growing seasons, and thus increased forest growth in many boreal regions (Pulliainen *et al.* 2017, Kellomäki *et al.* 2018), but also in intensified droughts (Peng *et al.* 2011) and other climate-related risks. Climate change affects the emissions of gases, such as BVOCs, by the forest, as well as atmospheric aerosol particle formation and growth through changing environmental conditions. Warmer temperatures and/or higher radiation levels promote photosynthesis (Hari *et al.* 2018), BVOC emissions (Loreto and Schnitzler 2010, Guenther *et al.* 2012, Yli-Juuti *et al.* 2021) and accumulation of aerosol particles to increase condensation sink (Paasonen *et al.* 2013), whilst decreasing moisture, i.e., soil moisture and ambient humidity, may be linked to decrease in BVOC release and the agglomeration rate of particles (Bonn *et al.* 2019). Studying past years with extreme weather events, such as exceptionally warm and dry summers, can help elucidate the boreal forest's response to climate change.

Our aim in this study is to describe and discuss the seasonal variation patterns of meteorological, ecosystem and atmospheric variables, as well as the correlation between these seasonal variation patterns. As data, we use the field measurements of emissions and concentrations of organic/inorganic gases and atmospheric aerosol particles between 1996 and 2020 at the SMEAR II (Station for Measuring Ecosystem — Atmosphere Relations; see Hari and Kulmala (2005) and Kulmala *et al.* (2021)) boreal forest site. We expect that an analysis of these long-term measurements will provide more robust insights into the seasonal interrelations of the ecosystem-atmosphere system, as compared with analyses based on shorter time scales.

In addition, to increase our understanding on the possible response of a boreal forest to continued global warming, we study two past summers, 2010 and 2018, with exceptionally high temperatures and signs of drought. The relationships between meteorological, ecosystem, and atmospheric variables give insight in the effects that dominate the response of the boreal forest to extreme events. To study the effects of extreme weather, we need long-term measurements to understand the baseline, as well as the extremes.

Material and methods

The data used for the analysis in this study was collected at SMEAR II, located in Hyytiälä, Southern Finland (61º51′N, 24º17′E, 181 m a.s.l.) and was retrieved from Smart-SMEAR (Junninen *et al.* 2009). The SMEAR II station is a rural background site surrounded by a boreal Scots pine forest with some understory and close by stands of Norway spruce. A more detailed overview of the measurement techniques employed at the SMEAR II station can be found in Hari and Kulmala (2005). The data collection at SMEAR II started in 1995. In this study, data collected in the period between 1 January 1996 and 31 December 2020 was analysed. At the end of the analysis period, the trees were 59 years old, and their average height was ~21 m. Figure 1 shows the coverage of the included data per instrument. Gaps in the included data result from instrument maintenance, winter measurement breaks, unprocessed recent data, and the choice for a specific measurement technique for data sets where the technique has changed over the years.

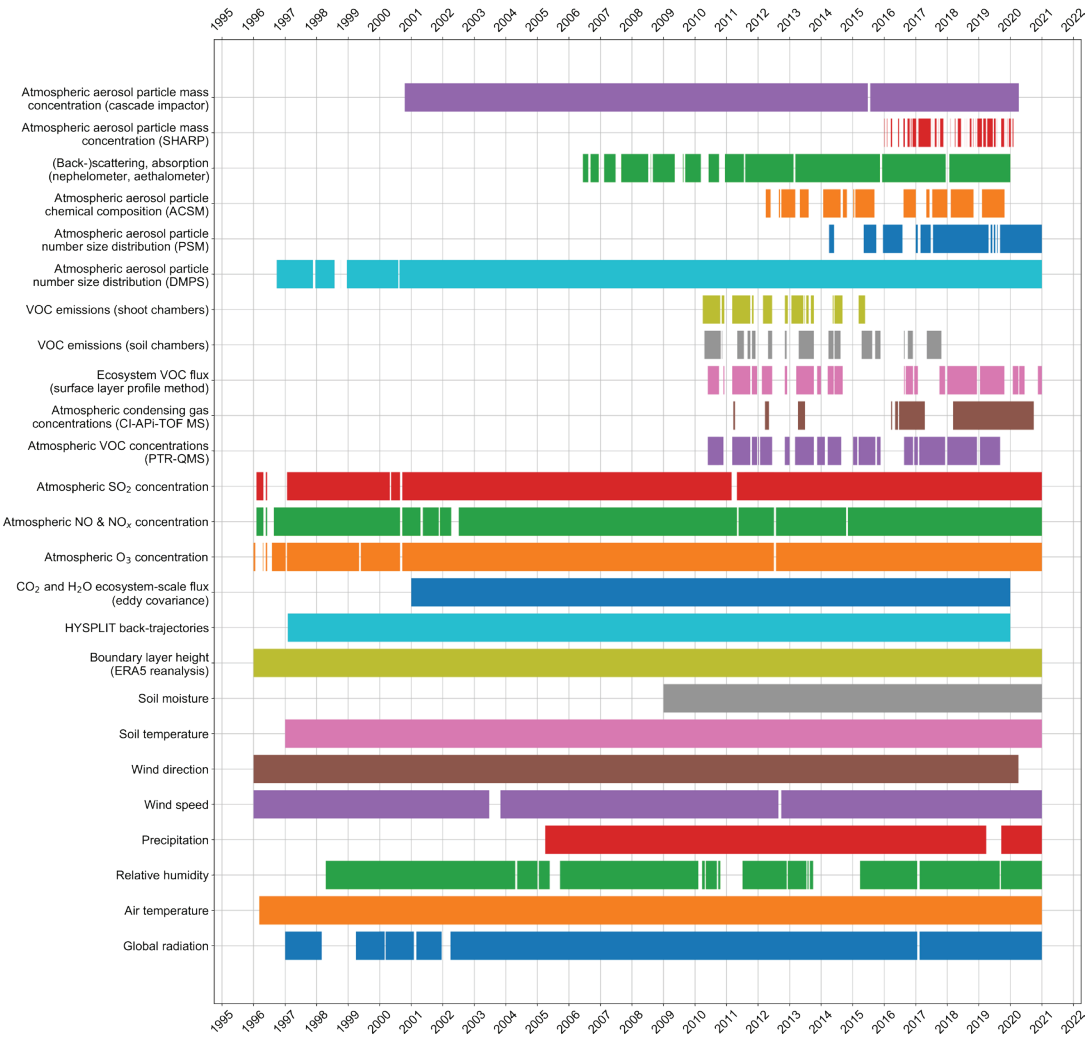

Fig. 1. Coverage of the data included in this study. For a specific instrument, a day is considered covered when at least 50% of its data points on that day exist. SHARP: Synchronised Hybrid Ambient Real-time Particulate monitor, ACSM: Aerosol Chemical Speciation Monitor, PSM: Particle Size Magnifier, DMPS: Differential Mobility Particle Sizer, CI-APi-TOF MS: chemical ionisation atmospheric pressure interface time-of-flight mass spectrometer, VOC: volatile organic compound, PTR-QMS: proton-transfer-reaction quadrupole mass spectrometer.

Meteorological and environmental data

Meteorological variables

Global radiation is measured as the incidence of solar radiation with a wavelength range from 0.3–4.8 µm. It was measured with a Reemann TP3 pyranometer (Astrodata, Estonia) from 1996 to June 2008, a Middleton SK08 pyranometer (Middleton Solar, Australia) from June 2008 to August 2017, and a Middleton EQ08 pyranometer (Middleton Solar, Australia) from August 2017 onward. Measurements were done above the canopy at a height of 18 m between 1996 and October 2017. In October 2017, the measurement height was moved to 35 m to account for the growth of the trees in the forest. The time resolution of global radiation measurements was 1 minute, and the unit is W m^{-2}.

Photosynthetically active radiation (PAR) is the wavelength range of solar radiation usable for photosynthesis (400–700 nm). It was meas-

ured with a Li-190SZ quantum sensor (LI-COR Biosciences, UK) for the whole studied period. Measurements were done above the canopy at a height of 18 m between 1996 and February 2017. In February 2017, the measurement height was moved to 35 m to account for the growth of the trees in the forest. The time resolution of PAR was 1 minute, and the unit is μmol m^{-2} s^{-1}.

Air temperature was measured with Pt100 sensors inside ventilated custom-made radiation shield for the whole studied period. Measurements were done at 15 different heights between 0.4 and 125 m. For this study, only the temperature measurements at 16.8 m (around the canopy) were used. The time resolution of air temperature was 1 minute, and the unit is ºC.

Relative humidity (RH) was calculated using data from dewpoint between April 1998 and May 2012, and measured with Rotronic MP102H RH sensors (Rotronic, Switzerland) from June 2012 onward. Measurements were done at 16-m height until January 2017 and then switched to 35-m height due to the growth of trees in the forest. The time resolution of RH was 1 minute, and the measurements are given in percentage.

Precipitation was measured as accumulated liquid water equivalent precipitation. It was measured with a Vaisala FD12P weather sensor (Vaisala, Finland) at 18-m height from April 2005 onward. The time resolution of precipitation was 1 minute, and the unit is millimetre (mm).

Wind speed and wind direction were measured with Vector A101M/L cup anemometers (Vector instruments, UK) between 1996 and September 2003, and with Thies 2D Ultrasonic anemometers (Thies Clima, Germany) from September 2003 onward. Measurements were done at 7 different heights between 4.2 m and 125 m over the whole studied period. For this study, wind direction is reported as an average of the heights: 16.8 m 33.6 m, and 67.2 m. The time resolution of wind speed and wind direction was 1 minute, and the units are m s^{-1} and degrees (º), respectively.

Soil temperature was measured in the organic layer of the soil surface as a mean of five locations. At the SMEAR II station, the organic layer is typically less than 5 cm deep. Measurements were done with a Philips KTY81-110 temperature sensor for the whole studied period. The time resolution of soil temperature was 15 min., and the unit is ºC.

Soil moisture was measured as the volumetric soil surface water content. It was measured with Tektronix reflectometer (Tektronix, USA) between May 1997 and December 2004, and with a TDR100 reflectometer (Campbell Scientific, USA) from January 2005 onward. Measurements were done in the organic layer of the soil surface (typically less than 5 cm deep). The time resolution of soil moisture measurement was 30 min., and the unit is volume of water per volume of soil (m^3 m^{-3}).

Vapour pressure deficit (VPD) was calculated using air temperature and RH (Alduchov and Eskridge, 1996; Monteith and Unsworth, 2014).

It is important to note that at the SMEAR II station, meteorological variables are not measured at the standard heights prescribed by the World Meteorological Organisation (WMO). The measurement heights rather reflect locations that are important for studying the interrelation between ecosystem and atmosphere (e.g., near the canopy or forest floor).

Boundary layer height

The boundary layer is the layer above the forest where vertical transports by turbulence play a dominant role in transfers of momentum, heat, moisture, and gases. Boundary layer height data was obtained from ERA5 reanalysis that is based on the Integrated Forecast System (IFS) from the European Centre for Medium-Range Weather Forecasts (ECMWF) (Hersbach *et al.* 2020). The ERA5 data has a grid resolution of 31 km. We utilised the grid point closest to Hyytiälä (61º, 24º17′E). For this study, the years 1996–2020 were included, although ERA5 reanalysis covers the period from 1950 to present. The time resolution of the ERA5 data was 1 hour and the unit of boundary layer height is measured in meters (m).

HYSPLIT trajectories

Air mass back trajectories give predictions on the origin of the air masses present above the forest.

We utilised 96-hour-long air mass back trajectories calculated for every hour with the Hybrid Single-Particle Lagrangian Integrated Trajectory model (HYSPLIT) by NOAA's Air Resources Laboratory (Stein *et al.* 2015) (available at https://www.ready.noaa.gov/HYSPLIT.php) for the years 1997–2020. The NCEP meteorological data sets (available at https://www.ready.noaa.gov/archives.php) used to run the model were the 1º FNL archive data for years 1997–2006, the 1º and 0.5º GDAS archive data for years 2007–2013 and 2014–2019, respectively, and finally the 0.25º GFS archive data for 2020. The trajectories were computed with arrival heights of 100 m above ground level in Hyytiälä, and they were grouped into three source regions: clean, Europe, and Russia (Fig. S1 in Supplementary Information) (Heikkinen *et al.* 2020a). The trajectory had to spend a minimum of 90% of the time in a sector before arriving in Hyytiälä, otherwise, it was labelled as "mixed".

Eddy covariance measurements

Net ecosystem exchange (NEE) of carbon dioxide (CO_2) between the atmosphere and the forest ecosystem and forest evapotranspiration (ET) was estimated using the eddy covariance (EC) technique that measures the covariance between the vertical wind speed, and CO_2 and H_2O concentrations. CO_2 and H_2O concentrations were measured with a LI-6262 infrared absorption gas analyser (LI-COR Biosciences, UK) between August 2001 to March 2018, and a LI-7200 infrared absorption gas analyser (LI-COR Biosciences, UK) from April 2018 onward. Vertical wind speed was measured with a Gill Solent 1012R anemometer (Gill Instruments, UK) between August 2001 to March 2018, and a Gill HS-50 anemometer (Gill Instruments, UK) from April 2018 onward. Measurements for both CO_2 and H_2O concentrations and vertical wind speed were done at 23-m height before March 2018 and at 27 m after March 2018. NEE was partitioned into total ecosystem respiration (RE) and gross primary production (GPP) using a method described e.g., in Kulmala *et al.* (2019). The time resolution for both NEE and ET measurements was 30 min., and the units are μmol CO_2 m^{-2} s^{-1} and mmol m^{-2} s^{-1}, respectively.

Volatile organic compound emission measurements

VOC emissions of the boreal forest at the SMEAR II field station were measured at three scales: ecosystem, forest floor, and Scots pine branches. At all three scales, the measurements were performed with a proton-transfer-reaction quadrupole mass spectrometer (PTR-QMS; Ionicon Analytik, Austria; Aalto *et al.* (2014)).

The VOC flux measurements at the ecosystem scale were collected continuously from May 2010 to the end of 2020 and calculated using the surface layer profile method, according to Rantala *et al.* (2014), from the measured VOC concentration profile. Turbulence parameters, including friction velocity and Monin-Obukhov length, used in the calculation were obtained from the EC measurement setup. Due to changes in the measurement setups, we used measurements from 23-m height until March 2018 and after that from 27-m height. The ecosystem flux was measured every third hour. Very stable (stability parameter $\zeta > 1$) and unstable ($\zeta < -2$) cases as well as cases with low friction velocity ($u_* \leq 0.2$ m s^{-1}) were filtered out from the ecosystem scale VOC flux data as these conditions might result in artificial flux values.

Forest floor VOC emission measurements were conducted during the snow-free seasons with three automated flow-through chambers (Aaltonen *et al.* 2013; Mäki *et al.* 2019). The VOC fluxes were calculated based on the VOC concentration change at the beginning (400 seconds) of the chamber measurement using a mass balance equation (Kolari *et al.* 2012). The locations of the forest floor chambers did not change during the measurement period from April 2010 to November 2017. The unit for both the ecosystem and forest floor flux measurements is nanogram per forest floor area per second (ng m^{-2} s^{-1}).

For measurements of the emissions from Scots pine branches, the PTR-QMS was connected to a cylinder chamber placed around tree branches. The measurements were made in two Scots pine trees for one- to two-year-old branches between March 2010 and May 2015. The unit for these measurements is nanogram per gram of needle dry weight per second (ng g^{-1} s^{-1}). The emissions from forest floor and

branches were measured hourly for maximum 16 hours per day (every third hour there is no data because the chamber lines were divided with several chambers).

Both isoprene and methylbutenol fragments are detected at m/z 69. Many pine species, including Scots pine, are known to emit more methylbutenol than isoprene (Zeidler and Lichtenthaler 2001, Tarvainen *et al.* 2005, Gray *et al.* 2006, Hakola *et al.* 2006, de Gouw and Warneke 2007). We therefore anticipate the emissions at the branch scale to be mainly composed of methylbutenol fragments. Rantala *et al.* (2015), however, concluded that for SMEAR II most of the m/z 69 signal at ecosystem scale can be attributed to isoprene, due to high summer emissions of isoprene from other tree species in the ecosystem footprint area, such as European aspen. The exact composition of the m/z 69 signal for forest floor emissions at SMEAR II is currently unknown. For consistency across the three scales, all emissions at signal m/z 69 were labelled "isoprene".

Atmospheric trace gas concentration measurements

Sulphur dioxide (SO_2) concentrations were measured with TEI 43B (1996–1/2004), TEI 43CTL (1/2004–9/2010), TEI 43iTL (9/2010 onward) UV fluorescence analysers from Thermo Fisher Scientific, USA. For nitric oxide (NO) and nitrogen oxides (NO_x) concentrations, TEI 43S (1996–8/1996), TEI 42CTL (8/1996–4/2011), and TEI 42iTL (5/2011 onward) chemiluminescence analysers from Thermo Fisher Scientific, USA, were employed. Ozone (O_3) concentration measurements were done with TEI 49 (1996–5/2004) and TEI 49C (5/2004 onward) UV photometric analysers from Thermo Fisher Scientific, USA. All these atmospheric trace gas concentrations were measured at 4.2-m height with a time resolution of 6 min., and unit parts per billion (ppb).

VOC concentrations were measured with a PTR-QMS (Ionicon Analytik, Austria; Taipale *et al.* (2008)) starting from 2007. Although the PTR-QMS technology allows the detection of many gases, we only used the data for isoprene and total monoterpene concentration respectively at m/z 69 and m/z 137. As with VOC emissions, both isoprene and methylbutenol fragments are detected at m/z 69. For consistency with the emission results, and in agreement with Rantala *et al.* (2015), we labelled all concentrations at signal m/z 69 as "isoprene". We considered measurements taken at 33.6 m. VOC concentrations are measured every third hour because the PTR-QMS measurements are allocated for measurements from forest floor and branch chambers for the other hours (Taipale *et al.* 2008). The unit is ppb.

Sulfuric acid (H_2SO_4), and highly oxygenated organic molecules (HOMs; Ehn *et al.* 2012, 2014, Bianchi *et al.* 2019) both play a role in the condensation of gas-phase molecules to atmospheric aerosol particles. They are, therefore, also referred to as condensing trace gases. These condensing trace gases were measured by a nitrate-based chemical ionisation atmospheric pressure interface time-of-flight mass spectrometer (NO_3^- CI-APi-TOF MS, TOFWERK, Switzerland). The instrument has been described earlier by Junninen *et al.* (2010) and Jokinen *et al.* (2012).

According to Jokinen *et al.* (2012), the total H_2SO_4 concentration can be calculated accounting for the (unit mass resolution) signal intensity at m/z 97 (HSO_4-) and m/z 160 ($H_2SO_4NO_3^-$). When using NO_3^- as charger ion, the sum of integrated signal is scaled to a coefficient determined by H_2SO_4 calibration after normalisation to the sum of reagent ion (here NO_3^- (m/z 62), $HNO_3NO_3^-$ (m/z 125) and $(HNO_3)2NO_3^-$ (m/z 188)). We estimated HOM concentrations separately for HOM monomers (i.e., C_{10} compounds) and HOM dimers (i.e., C_{20} compounds) as the sum of signals between m/z 290 and 430 and between m/z 430 and 620, respectively. The total HOM concentration is the sum of HOM monomer and HOM dimer, normalised to NO_3^- multimer ions and scaled with the instrument specific calibration coefficient calculated for H_2SO_4.

Originally, CI-APi-TOF was used at SMEAR II station during summer campaigns (in 2011, 2012, 2013 and 2016). From 2018, the measurements were changed to continuous measurements throughout the year. The instrument sampled either from the ground (1-m high inlet) or at

canopy level (35-m tower). Ground level HOM characterization from Hyytiälä can be found in Yan *et al.* (2016) and the results of parallel/simultaneous measurements with (CI)-APi-TOF from both ground and tower levels are reported in Zha *et al.* (2018). Zha *et al.* (2018) found HOM concentrations to be similar between the ground and tower level during the daytime, while larger differences occur during night-time. When the surface micro-meteorology is stable both measurements are highly comparable. However, when temperature inversion phenomena occur — typically during the later summer months — the measurement show discrepancies that are difficult to comprehensively assess and correct for. Herein, we combined both ground and tower data into one data set to improve the data coverage included in our work, since they still provide the best estimates available and considering that our study mostly compares range of magnitudes. The time resolution of the CI-APi-TOF MS was 2 min. and the unit is particles per cm^3 (cm^{-3}).

Atmospheric aerosol particle concentration measurements

When studying the effects of atmospheric aerosol particles on air quality, both the number of particles (number concentration) and the mass of the particles (mass concentration) are important quantities. The number concentration of submicron size atmospheric aerosol particles was measured with two different types of instruments. Differential Mobility Particle Sizers (DMPS; University of Helsinki, Finland) were used to measure the number concentrations of atmospheric aerosol particles in the size range of 3 to 1000 nm during the whole studied period. The SMEAR II station's twin-DMPS system is described in detail in Aalto *et al.* (2001). The size range of the DMPS measurements was further divided into three classes, representing the nucleation mode (3–25 nm), Aitken mode (25–100 nm), and accumulation mode (100–1000 nm) particle sizes. A Particle Size Magnifier (PSM; Airmodus, Finland; Vanhanen *et al.* 2011) was used to measure the number concentration of atmospheric aerosol particles in the size range 1 to 3 nm starting in April 2014 onward. For this study, only the concentrations of sub-2-nm particles were analysed. Time resolutions of particle concentration measurements differed between instruments, as well as within the data period analysed, and ranged from 2–15 minutes. For further analysis, all the measurements were aggregated to an hourly level using the median of sub-hourly measurements. DMPS and PSM measurements were performed at 8 m and 1.6 m, respectively. The unit of number concentration is particles per cm^3 (cm^{-3}).

Mass concentrations, or particulate mass (PM), of atmospheric aerosol particles with diameter smaller than 1 μm (PM1), 2.5 μm (PM2.5), and 10 μm (PM10) were measured through particulate sampling with a gravimetric cascade impactor (Dekati, Finland; Keskinen *et al.* 2020) from October 2010 onward. Cascade impactor measurements were done at 5-m height. The collected particulate samples were weighted every two or three days. For this study, the data was converted to daily time resolution. From January 2016 onward, mass concentrations of PM10 were also measured continuously with the Synchronised Hybrid Ambient Real-time Particulate monitor (SHARP; Thermo Fisher Scientific, USA; Keskinen *et al.* 2020). SHARP measurements were performed at 6-m height within the canopy. The original time resolution was 1 second, but the data was averaged over one hour. The unit of mass concentration is $\mu g\ m^{-3}$. The cascade impactor measures PM10 through sampling while SHARP measures PM10 continuously. Both measurements are maintained to ensure good quality and comparison (Keskinen *et al.* 2016).

A NPF event day is defined as a day where clear formation of new 3–25 nm atmospheric aerosol particles, and their subsequent growth, took place. If no NPF was observed, the day was classified as a non-event day. Days for which it was not possible to reliably discern if NPF had occurred or not, were classified as undefined days. The classification was made using the DMPS atmospheric aerosol particle number concentration measurements and was based on criteria by Dal Maso *et al.* (2005).

Condensation sink (CS) is the inverse lifetime of a non-volatile vapour against condensation onto pre-existing aerosol particles. Conventionally, CS is defined by assuming the vapour

to be H_2SO_4. However, even when CS is defined for H_2SO_4, it is also related to the loss of small ions and clusters, i.e., newly formed atmospheric aerosol particles. It has been shown that CS values are mainly determined by accumulation mode atmospheric aerosol particles (Nieminen *et al.* 2014). CS was calculated using the DMPS atmospheric aerosol particle number concentration measurements according to (Kulmala *et al.* 2012).

Atmospheric aerosol particle chemical composition measurements

The chemical composition of atmospheric aerosol particles is estimated by measuring the mass concentration of total organics, sulphate (SO_4^{2-}), nitrate (NO_3^-), ammonium (NH_4^+) and chloride (Cl^-). Measurements were done with an Aerosol Chemical Speciation Monitor (ACSM, Aerodyne) from March 2012 onward at 4-m height within the canopy. For this study, particles larger than 2.5 μm were filtered out before the measurements (Heikkinen *et al.* 2020b). The time resolution of atmospheric aerosol particle chemical composition measurements was 1 hour, and the unit is μg m^{-3}.

Aerosol optical properties

The measurements of aerosol optical properties (AOPs) included measurements of light scattering, backscattering, and absorption coefficient. Scattering measurements were conducted at three wavelengths (450, 550, and 700 nm) with a TSI 3563 integrating nephelometer (TSI Incorporated, USA). Absorption measurements were conducted at seven wavelengths (370, 470, 520, 590, 660, 880, and 950 nm) with a AE31 aethalometer from June 2016 to December 2018 and AE33 aethalometer from January 2019 onward (both aethalometers from Magee Scientific, USA; Luoma *et al.* 2019). Aerosol optical properties measurements were done at 5-m height. Here, we used data measured at green wavelength (550 nm for scattering data and 520 nm for absorption data). Equivalent black carbon (eBC) concentration is defined as the black carbon (e.g., soot) concentration derived from optical measurements. In this study, eBC was obtained from the absorption coefficient at 880 nm (Petzold *et al.* 2013). The time resolution of AOP data was 1 hour, and the unit is Mm^{-1} for scattering, backscattering and absorption coefficients, and μg m^{-3} for eBC.

Analysis methods

For each variable in this study, the data was analysed on a monthly scale. First, the monthly medians were computed separately for each year. These single-year monthly medians were only computed if at least 50% of the data was available for that month, except in the case of atmospheric aerosol particle chemical composition where the inclusion limit was set at 33% due to the measurement frequency of that data. We subsequently computed the monthly median over all the years in the measurement period by taking the median of the single-year monthly medians. Interquartile ranges (25th and 75th percentiles) were also calculated from the single-year monthly medians over all the years in the measurement period. For precipitation, the monthly values for single years were computed as monthly accumulated precipitation. For wind direction data, the monthly values were computed as circular medians.

The links between variables and environmental conditions were investigated with scatter plots and by computing Pearson correlation coefficients (or short *r*) between the variables utilising the monthly medians.

For selected variables, a median diurnal cycle analysis was conducted. The diurnal analysis was performed separately for each season: winter as December-January-February (DJF), spring as March-April-May (MAM), summer as June-July-August (JJA), and autumn as September-October-November (SON).

Results and discussion

In the following sections, we report, compare, and discuss the seasonal variation of: (1) the meteorological conditions; (2) carbon

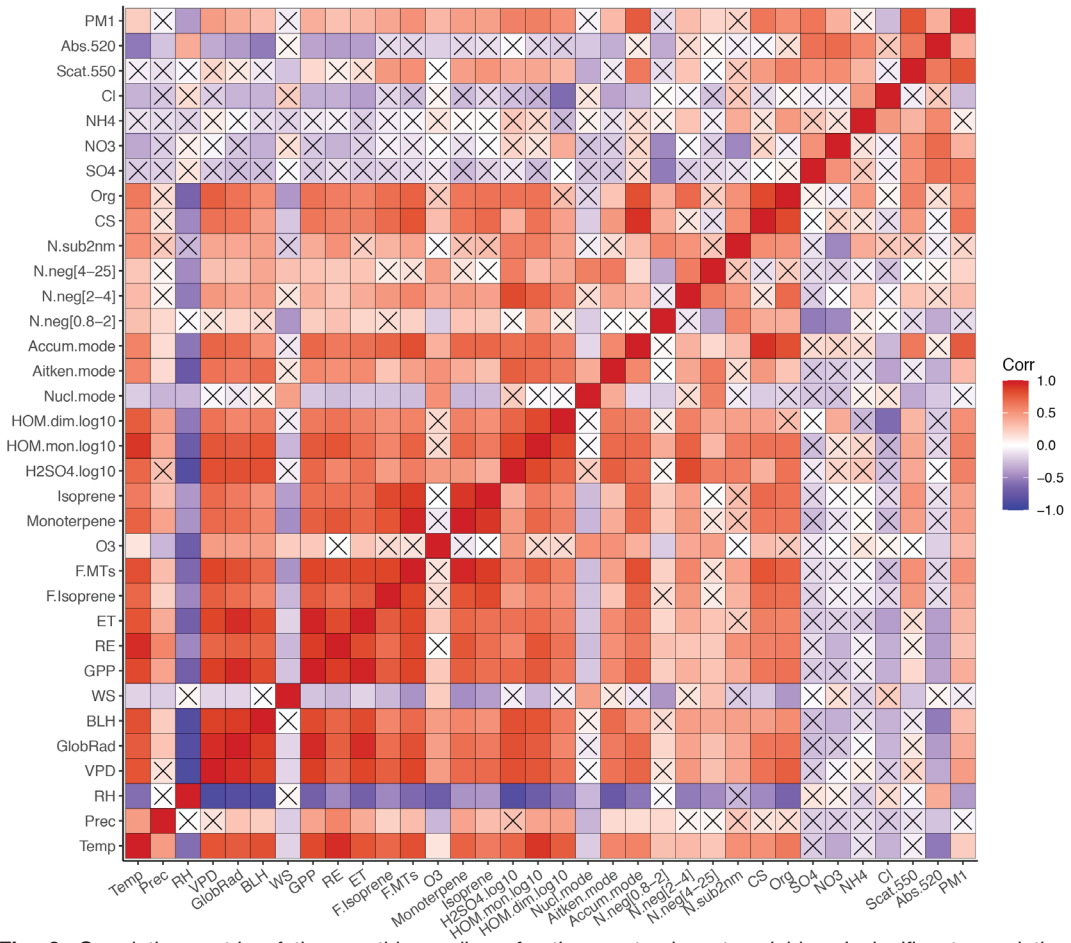

Fig. 2. Correlation matrix of the monthly medians for the most relevant variables. Insignificant correlations (p-value > 0.05) are marked with a cross. For the full names of the abbreviations and shortened variable names, see Table S1 in the Supplementary Information. The concentrations of condensing trace gases H_2SO_4, HOM monomer and dimer are given in log-scale.

and water exchange between the forest ecosystem and the atmosphere; (3) VOC emissions; (4) atmospheric trace gas concentrations; (5) atmospheric aerosol number concentrations and related variables; and (6) atmospheric aerosol mass concentration, chemical composition, and optical properties, between the years 1996 and 2021 at the SMEAR II station. In doing so, we follow the trajectory from forest emissions to eventual atmospheric aerosol particle formation and growth. After discussing the meteorological conditions, each subsequent section is divided in a discussion of the monthly variation of the variables and a discussion of the links between the variables and the meteorological conditions.

Figure 2 presents an overview of the monthly correlations between the most relevant meteorological variables, ecosystem-level fluxes and concentrations, and aerosol properties. The Pearson correlation coefficients were calculated from the pairwise complete data. To save space and increase readability, we left out some variables that, for example, are derived from other variables (e.g., equivalent black carbon), show similar correlations to the variables included in the matrix (e.g., global radiation and PAR, and air and soil temperatures) or are known not to be linearly correlated with other variables (e.g., soil moisture). Most of the correlations seem to be significantly positive,

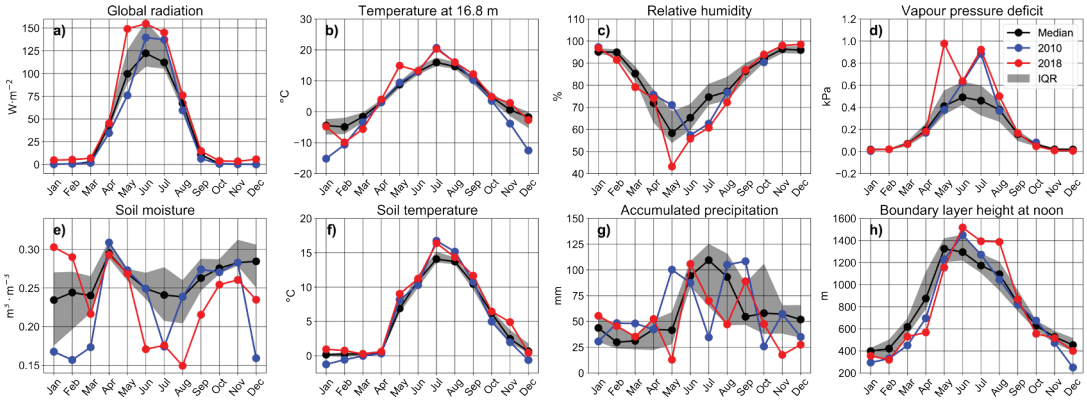

Fig. 3. Monthly medians of (**a**) global radiation (1997–2020); (**b**) air temperature at 16.8-m height (1996–2020); (**c**) relative humidity (1998–2020); (**d**) vapour pressure deficit (1998–2020); (**e**) soil moisture (organic layer; 2009–2020); (**f**) soil temperature (organic layer; 1997–2020); (**g**) accumulated precipitation (2005–2020); and (**h**) boundary layer height at noon (1996–2020). The medians of monthly medians over all years are shown in black and interquartile range (IQR) in grey shading. Monthly medians of the years 2010 and 2018 are shown in blue and red, respectively. For precipitation, the monthly values of single years are the monthly values of accumulated precipitation.

although negative correlations occur especially for RH, wind speed, and nucleation mode particle concentrations. In addition, concentrations of inorganic aerosol species (NH_4^+, NO_3^-, SO_4^{2-}, Cl^-) do not seem to correlate significantly with most other variables, but this could partly be caused by short data periods and variations of the correlations depending on the season (summer vs. winter). The correlations and links between different variables are discussed in more detail in the following sections.

Meteorological and environmental conditions

Yearly cycles of global radiation, air temperature, accumulated precipitation, soil moisture and temperature in the organic layer, relative humidity, vapour pressure deficit and boundary layer height are presented with monthly medians over all studied years in Fig. 3. After comparing the monthly medians of different years (not shown), we selected two years, 2010 and 2018, to be studied in more detail. The summer months of these years are characterised by high air and soil temperatures and more global radiation than the median over all the studied years. Furthermore, the soil moisture content in summers 2010 and 2018 was significantly lower than the median over all years.

The global radiation as well as air and soil temperatures naturally have their maximum values in summer and minimum in winter (Fig. 3a,b,f). The monthly median air temperature was above 0ºC from April to October. The warmest month was July, with a median air temperature of 15.9ºC, and the coldest was February, with a median air temperature of –4.9ºC. The median soil temperature was the lowest, 0.2ºC, in January, and the highest, 14ºC, in July.

In 2010, the global radiation was lower than usual in April and May and higher than usual in June and July, whereas in 2018, the global radiation was higher than usual in May–July. This was reflected in air and soil temperatures, which were mostly higher than usual during May–August in both years. Both in 2010 and 2018, the winter was colder than usual, whereas November 2018 was slightly warmer than usual.

When looking at the medians of monthly accumulated precipitation over the whole measurement period of 2005–2020, the precipitation was highest, 109 mm, in July and lowest, 30 mm, in February (Fig. 3g). Compared with the median over all years, the year 2010 had more precipitation in spring and autumn and

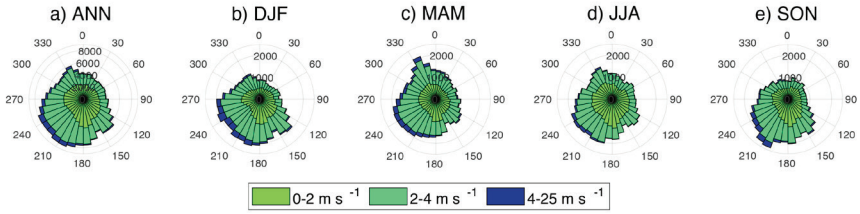

Fig. 4. Wind roses of hourly wind speeds and wind directions (**a**) annually (ANN) and during (**b**) winter (DJF), (**c**) spring (MAM), (**d**) summer (JJA), and (**e**) autumn (SON) seasons. The counts of wind speed classes are noted within the wind roses. Data from years 1996–2020 is included.

less precipitation in summer. The year 2018, on the other hand, had less precipitation than usual in May, July, August, and late autumn and more precipitation than usual in September.

The monthly median soil moisture was lowest in late winter and summer, approximately 0.23 m^3 m^{-3}, and highest in April and late autumn, up to 0.29 m^3 m^{-3} (Fig. 3e). The April peak is linked to melting snow, while the Autumn peak likely comes from the decreased uptake of water by the vegetation. In 2010, both winter and summer were drier than the median over all years, the median soil moisture being 0.16 m^3 m^{-3} at the lowest. In 2018, the monthly median soil moisture was lower than usual in summer and autumn, being as low as 0.15 m^3 m^{-3} in August.

RH was highest in winter, with a monthly median of 96% in December, and lowest in late spring, with a monthly median of 58% in May. Following the same pattern as precipitation, RH was higher than usual in May 2010, and lower than usual in June and July 2010. In 2018, the summer was even drier than in 2010, with the lowest values of median RH, 43%, seen in May.

VPD was highest in summer, with a monthly median of 0.5 kPa in June, and lowest in winter, with a monthly median of 0.02 kPa in December (Fig. 3d). During the warm and dry summers of 2010 and 2018, VPD was higher than usual, as would be expected, being as high as 0.98 kPa in May 2018.

The boundary layer height at noon was shallower during winter (around 400 m) compared with the summer when it had its yearly maximum value, 1300 m (Fig. 3h). There was, furthermore, a clear diurnal pattern in summer and a flatter pattern in winter (Fig. S2 in Supplementary Information), similarly as in Sinclair *et al.* (2021). In 2010 and 2018, the boundary layer height at noon was higher than usual in summer, likely due to higher sensible heat flux (buoyancy flux) during hot and dry summers. The boundary layer height depends on the atmospheric stability. If conditions are unstable, air rises and becomes well mixed. In stable conditions, mixing happens closer to the ground due to suppressed turbulence. At noon, the boundary layer is more often unstable during May–June which explains the higher boundary layer heights observed in the same period in Hyytiälä (Manninen *et al.* 2018).

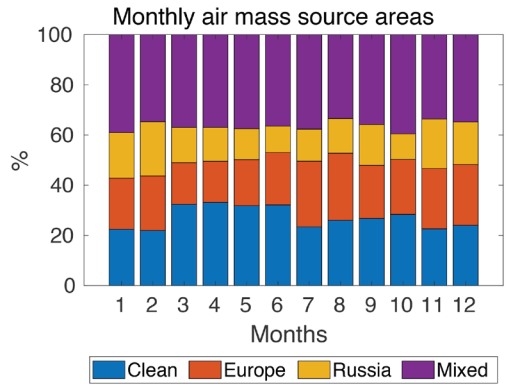

Fig. 5. Annual cycle of the source areas of air masses coming to Hyytiälä. Data from years 1997–2021 is included

The main wind direction in Hyytiälä was from the south-west and the wind speeds were most often below 4 m s^{-1} (Fig. 4). The monthly median wind speed had its maximum in wintertime, but the diurnal cycle was stronger during summer (Fig. S3 in Supplementary Information). During the winter season (DJF), winds mostly arrived from the southern direction. In spring and summer, there was an influence of

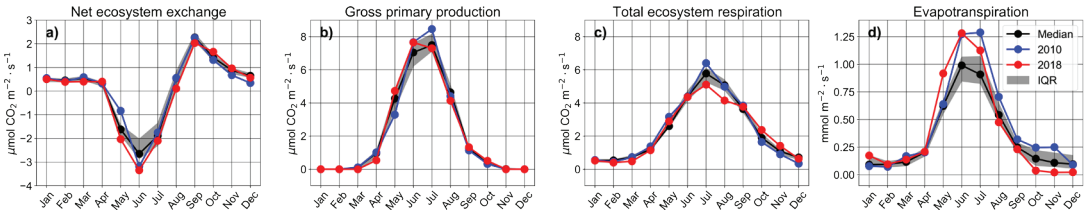

Fig. 6. Monthly medians of (**a**) net ecosystem exchange (NEE); (**b**) gross primary production (GPP); (**c**) ecosystem respiration (RE); and (**d**) evapotranspiration (ET). The medians of monthly medians over all years are shown in black with interquartile range (IQR) in grey shading. Monthly medians of years 2010 and 2018 are shown in blue and red, respectively. Data coverage of all four variables is 2001–2020.

north-westerly winds. During autumn, the most common wind direction was the south-west.

Based on the trajectory data, the majority of air masses crossed many sectors before arriving at Hyytiälä (Fig. 5). The air masses coming from Europe and Russia can be considered polluted whereas air masses coming from the north-west direction are expected to be cleaner (e.g., Heikkinen *et al.* 2020a). In February, there was an increased frequency of air masses coming from Russia, while a higher influence of European air masses was visible in July and August. More clean air arrived at Hyytiälä between March and June.

Carbon and water fluxes between ecosystem and atmosphere

Monthly variation

Annual cycles of carbon and water fluxes between the ecosystem and the atmosphere are shown in Fig. 6. The monthly median of NEE was negative from May to July (monthly mean NEE was negative from April to September, see Fig. S4 in Supplementary Information), indicating that the forest ecosystem was a median carbon sink in those months. During this period, GPP exceeded RE. The monthly median carbon sink was largest in June, being –2.64 μmol CO_2 m^{-2} s^{-1}. Monthly median GPP was highest in July, being 7.49 μmol CO_2 m^{-2} s^{-1} but then median RE was also at its highest, 5.78 μmol CO_2 m^{-2} s^{-1}, resulting in lower median NEE than in June (monthly mean GPP and RE were highest in July, Fig. S4 in Supplementary Information).

From August to April, monthly median NEE was positive, indicating that there was a median release of carbon to the atmosphere in these months. The monthly mean NEE was positive for a shorter time, from October to March (Fig. S4 in Supplementary Information). This difference is due to the median not being affected by the low day-time values of NEE like the mean is. The monthly median rate of carbon release to the atmosphere was highest, 2.26 μmol CO_2 m^{-2} s^{-1}, in September when RE was still relatively high, 3.63 μmol CO_2 m^{-2} s^{-1}, but GPP was already low, 1.27 μmol CO_2 m^{-2} s^{-1} (the monthly mean rate of carbon release was highest in October, Fig. S4 in Supplementary Information). From November to February, monthly median GPP was at zero and RE varied between 0.52 μmol CO_2 m^{-2} s^{-1} and 1.09 μmol CO_2 m^{-2} s^{-1}. During this winter dormancy period, monthly median NEE was between 0.45 and 0.88 μmol CO_2 m^{-2} s^{-1}.

In 2010, GPP was lower than the monthly median over all years in May and higher in June and July. RE, on the other hand, was higher than median in May and July. As a result, the uptake of carbon in 2010 was lower than the monthly median over all years in May, with median NEE being –0.83 μmol CO_2 m^{-2} s^{-1}, and higher in June, with median NEE being –3.18 μmol CO_2 m^{-2} s^{-1}.

In 2018, GPP was higher than the monthly median over all years in May and June and lower in August, but otherwise near the median values. RE, on the other hand, was lower than the monthly median over all years in July and August. As a result, the uptake of carbon in 2018 was higher than the monthly median over all years in May–July, with median NEE

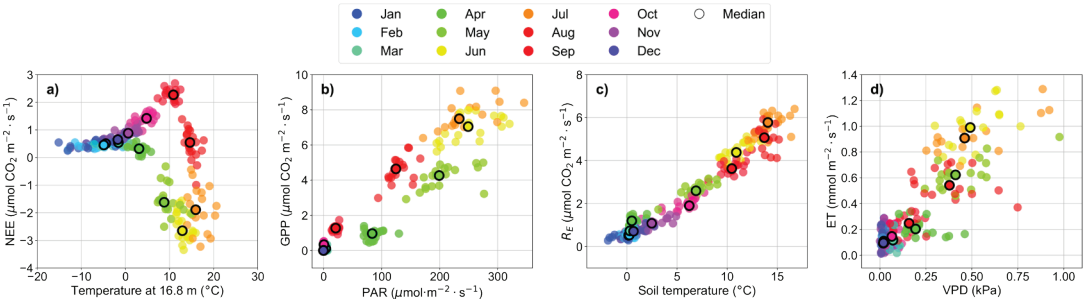

Fig. 7. (**a**) Net ecosystem exchange (NEE) vs. air temperature at 16.8-m height; (**b**) gross primary production (GPP) vs. photosynthetically active radiation (PAR); (**c**) ecosystem respiration (RE) vs. soil temperature; and (**d**) evapotranspiration (ET) vs. vapour pressure deficit (VPD). Monthly medians of single years are indicated with different colours and the medians of monthly medians over all years are indicated with black outline. Data from years 2001–2019 is included.

being between –3.34 μmol CO_2 m^{-2} s^{-1} and –2.03 μmol CO_2 m^{-2} s^{-1}. High temperature increases photosynthesis more than respiration in spring, whereas in autumn respiration increases more than photosynthesis due to high temperature (Piao *et al.* 2008; Wu *et al.* 2013). This can to a large extent be explained by plant phenology (Richardson *et al.* 2010; Wu *et al.* 2013). Also, as soil water content is typically not a limiting factor for GPP in spring, the warm spring and early summer in 2018 led to high GPP and NEE, whereas the warm and dry summer explains lower GPP later in the summer (Wang *et al.* 2020). However, it needs to be noted that at annual scale, the net carbon uptake of the studied site was slightly higher, especially in the warm and dry year 2018, than normal.

The monthly median of ET (Fig. 6d) was at maximum in June, 0.99 mmol m^{-2} s^{-1}, and minimum in December, 0.09 mmol m^{-2} s^{-1} (the monthly mean ET was at maximum in July, Fig. S4 in Supplementary Information). In 2010, ET was higher than the monthly median over all years in June–November, with the highest monthly median, 1.29 mmol m^{-2} s^{-1}, in July. In 2018, on the other hand, ET was higher than the monthly medians over all years in May–July and lower in October–December. At annual scale, ET of the studied site was higher in these warm and dry years compared with the median over all years. This indicates that the forest could cope well with the warm summer and maintained even higher ET rates than normally. Even if ecosystem surface conductance would be decreased due to plants keeping the stomata in leaves more closed during dry and warm summers compared with median summers, the increase in evaporative demand during a dry and warm summer can counteract this leading to increased transpiration per unit stomatal conductance.

Links with environmental factors

The dependence of NEE on air temperature shows an expected seasonal variation (Fig. 7a): NEE decreases exponentially with temperature during spring and summer, increases with decreasing temperature in August and decreases exponentially with decreasing temperatures during autumn. The two components of NEE, gross primary production and respiration, are regulated by different environmental factors and the dependencies are not always linear (e.g., Baldocchi *et al.* 2018). With a given temperature, we see higher ecosystem uptake of carbon (i.e., more negative NEE) in spring than in autumn (Fig. 7a). As respiration is similarly dependent on temperature throughout the year (Fig. 7c), this difference is explained by seasonal difference in the level of GPP per given temperature (Fig. S5b in Supplementary Information). This is in turn partly explained by GPP being dependent on radiation which has different quantities in spring and autumn, but most of all this difference can be explained by

plant phenology (Richardson *et al.* 2010; Wu *et al.* 2013). Correlations of the ecosystem fluxes and the different environmental parameters on a seasonal scale are presented in Fig. 2.

GPP shows clear seasonal correlation with PAR (Fig. 7b; Pearson's r = 0.95) and air temperature (Fig. S5b in Supplementary Information; r = 0.83) as the solar radiation drives photosynthesis at short timescale and air temperature in seasonal time scale through the state of the photosynthetic machinery (Hari *et al.* 2017). It is interesting to note that in the spring months (March–May), higher PAR values are required to obtain the same GPP as later in the growing season (Fig. 7b), which is due to the comparatively lower temperature in spring and the phenological transition from dormancy to spring recovery (Hari *et al.* 2017). On a seasonal scale, GPP is also positively correlated with VPD (Fig. S6b in Supplementary Information; r = 0.87), as the monthly median of VPD is highest in the warmest months. On an hourly scale, however, in dry conditions when VPD gets too high and soil moisture too low, photosynthesis decreases because the plants close the stomata to minimise water loss (e.g., Baldocchi *et al.* 2018; Grossiord *et al.* 2020). This can be seen in the median diurnal cycles: in summer 2018, the soil is exceptionally dry and when VPD increases during the day (Fig. S7d,e in Supplementary Information), GPP decreases below the median values over all years around noon and in the early afternoon (Fig. S8b in Supplementary Information).

Respiration (RE) increases with increasing air temperature (Fig. S5c in Supplementary Information; r = 0.93) and soil temperature (Fig. 7c; r = 0.97) which is expected because air and soil temperatures are among the variables used when partitioning NEE into GPP and RE. RE is also regulated by soil moisture (Fig. S9c in Supplementary Information) so that in too dry conditions, RE starts to decrease (e.g., Baldocchi *et al.* 2018). Dry soil is likely one affecting factor in the lower rate of RE observed in summer 2018, as soil moisture was also below average that summer (Figs. 3e and 6c). Lower soil moisture can also explain the lower GPP in July 2018 compared with 2010. Previous studies have shown that the drought in summer 2018 affected a large part of central and north-western Europe and reduced the rates of GPP, RE and carbon uptake in the region (e.g., Smith *et al.* 2020).

ET is correlated with air temperature (Fig. S5d in Supplementary Information; r = 0.79) and VPD (Fig. 7d; r = 0.85). It is also affected by soil moisture (Fig. S9d in Supplementary Information) because plants close their stomata to minimise water loss during dry periods. Launiainen *et al.* (2010) found that transpiration in the forest in Hyytiälä reduces strongly when soil moisture decreases below approximately 0.15 $m^3\ m^{-3}$. During our study period, soil moisture was lower than this threshold in August 2018 (Fig. 3e), when ET was also below the monthly median over all years (Fig. 6d).

BVOC emissions at ecosystem, branch, and forest floor scale

Monthly variation

The monthly median ecosystem-scale flux of isoprene at SMEAR II ranged from –0.09 ng $m^{-2}\ s^{-1}$ to 7.5 ng $m^{-2}\ s^{-1}$, whilst monthly median monoterpene flux was considerably higher and varied between 1.5 ng $m^{-2}\ s^{-1}$ and 71 ng $m^{-2}\ s^{-1}$ (Fig. 8a,d). This is in line with Rantala *et al.* (2015), who in a detailed analysis of the ecosystem scale BVOC fluxes at SMEAR II concluded that isoprene was only detected in summer months whereas monoterpene flux at SMEAR II was significant for most of the year. Rantala *et al.* (2015) reported that the highest monthly average fluxes in July were 18 ng $m^{-2}\ s^{-1}$ and 94 ng $m^{-2}\ s^{-1}$ for isoprene and monoterpenes, respectively. This is higher than our monthly median values, but within the range if we consider the extreme year 2018 (16 ng $m^{-2}\ s^{-1}$ and 144 ng $m^{-2}\ s^{-1}$ in July for isoprene and monoterpenes, respectively; Fig. 8a,d). The maximum ecosystem scale fluxes in 2010 and 2018 were 1.2–3 times higher than the long-term medians and reflect the anomalous temperature events compared with the long-term medians.

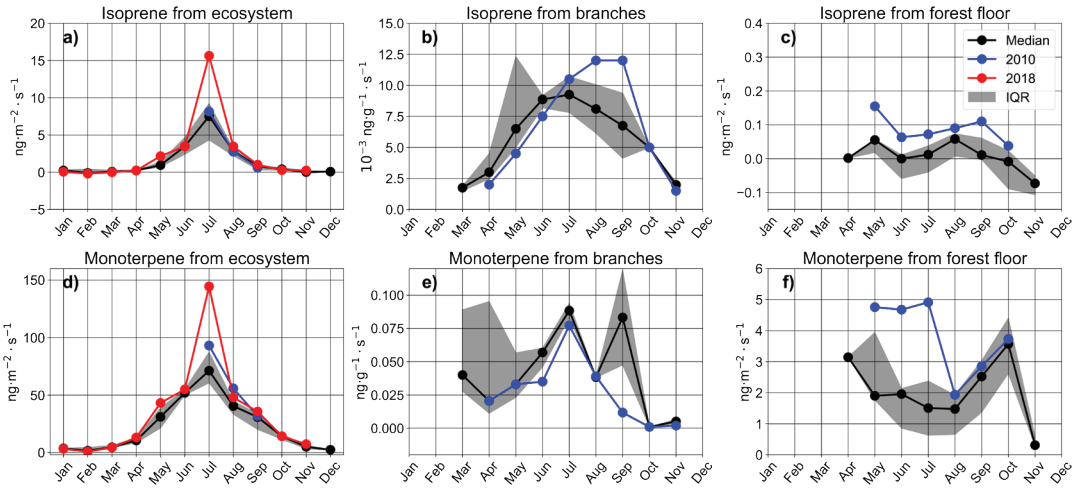

Fig. 8. Monthly medians of isoprene and monoterpene fluxes from (**a**,**d**) boreal ecosystem (2010–2020); (**b**,**e**) Scots pine branches (2010–2015), and (**c**, **f**) forest floor (2010–2017). The medians of monthly medians over all years are shown in black with interquartile range (IQR) in grey shading. Monthly medians of years 2010 and 2018 are shown in blue and red, respectively.

In our data, weak deposition of isoprene was observed in the cold and snow-cover period (the lowest monthly median isoprene flux was –0.09 ng m^{-2} s^{-1} (Fig. 8a)). Minor deposition has earlier been reported by Rantala *et al.* (2015) for ecosystem scale isoprene fluxes. The conditions when BVOC deposition takes place warrant further investigation, but it is possible that the isoprenoids may be absorbed into wet forest floor or snowpack and consumed by microbes (Aaltonen *et al.* 2012).

The highest monthly median emissions of isoprene and monoterpenes from Scots pine branches took place in summer months. The isoprene emissions were very small (ranged from 0.002 ng g^{-1} s^{-1} to 0.009 ng g^{-1} s^{-1}, Fig. 8b), and very likely the measured signal was not isoprene but methylbutenol fragments (e.g., Tarvainen *et al.* 2005). Monthly median monoterpene emissions from branches ranged between zero and 0.088 ng g^{-1} s^{-1} (Fig. 8e), with only minor differences between the long-term median and the warm year 2010.

The monthly median monoterpene emissions from the forest floor peaked in spring and autumn (3.1-3.6 ng m^{-2} s^{-1}; Fig. 8f). Our results agree with the previous studies by Aaltonen *et al.* (2012) and Hellen *et al.* (2006), who showed that the first peak in forest floor emissions during spring and early summer originates from compounds stored in and below the snowpack and are released after the snowmelt. For the second peak in autumn, decaying needle litter and fine roots on the forest floor are likely the main reasons for high monoterpene emissions (Janson, 1993, Hellén *et al.* 2006, Aaltonen *et al.* 2011, Mäki *et al.* 2017, 2019b). Like the branch measurements, isoprene emissions from forest floor were very small (Fig. 8c).

The effect of the warm and dry years to monthly median BVOC emissions were minor. The seasonal variations in BVOC emissions from evergreen branches are well documented (e.g., Tarvainen *et al.* 2005, Hakola *et al.* 2006). Incident temperature is the main driver for the monoterpene emissions from Scots pine branches (Hakola *et al.* 2012), however also photosynthetic capacity has been suggested to play a role in the emission onset and dynamics in spring and summer (Aalto *et al.* 2015; Vanhatalo *et al.* 2018). Higher than normal emission rates were detected with forest floor isoprene and monoterpene emission measurements in the warm summer 2010 (Fig. 8c,f).

Both isoprene and monoterpene fluxes at the ecosystem scale showed high seasonal

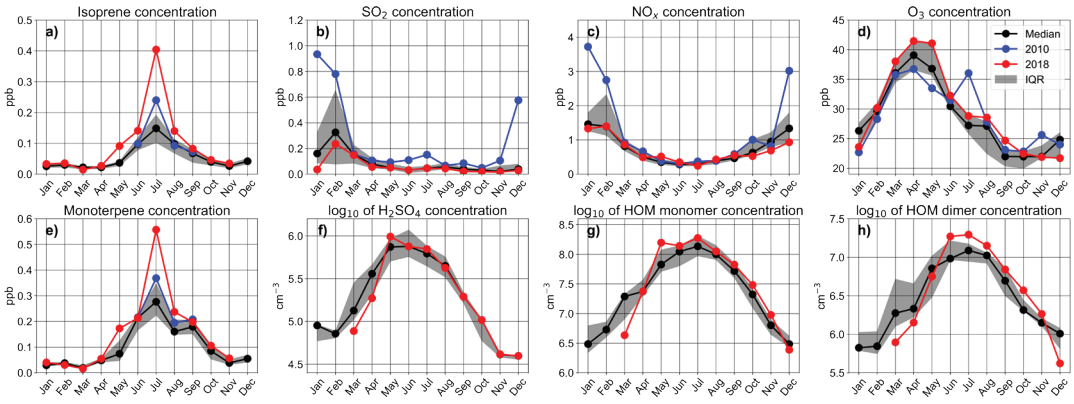

Fig. 9. Monthly medians of (**a**) isoprene (2010–2019); (**b**) SO_2 (1996–2020); (**c**) NO_x (1996–2020); (**d**) O_3 (1996–2020); (**e**) monoterpene (2010–2019); (**f**) $\log_{10}$ of H2SO4 (2011–2020); (**g**) $\log_{10}$ of HOM monomer (2011–2020); and (**h**) $\log_{10}$ of HOM dimer concentrations (2011–2020). The medians of monthly medians over all years are shown in black with interquartile range (IQR) in grey shading. Monthly medians of years 2010 and 2018 are shown in blue and red, respectively.

correlations ($r > 0.75$) with GPP, which is expected as higher GPP suggests more vegetation activity which is linked to the production of BVOCs (Guenther *et al.* 1995).

Links with environmental factors

The monthly median ecosystem fluxes of isoprene and monoterpenes correlated positively with air temperature (Fig. 2). The 3-hourly BVOC emissions from Scots pine branches, forest floor and ecosystem level showed better correlations with PAR than with air temperature or RH (Fig. S10a,b,c in Supplementary Information). The diurnal pattern of BVOCs from the three scales coincided with PAR variation before midday, but later in the afternoon and evening the emissions declined slower than PAR changed. Such an effect is likely correlated with temperature effects on the pool emissions (Fig. S10e–h in Supplementary Information) (e.g., Taipale *et al.* 2011, Rantala *et al.* 2015). Temperature is the dominant factor controlling monoterpene emissions from ecosystems via the physical effect on volatilisation from different pools (e.g., Niinemets *et al.* 2004, Hakola *et al.* 2006, 2017), but especially for isoprene emissions, light also plays an important role (e.g., Guenther *et al.* 1995). Unfortunately, further analysis of the relative importance of PAR and temperature on diurnal emission patterns was not possible due to the time scale of these data sets.

Atmospheric trace gas concentrations

Monthly variation

The monthly median concentrations of SO_2, NO_x, and O_3 are shown in Fig. 9b,c,d. SO_2 and NO_x had a concentration high in winter (maximum in February) and a concentration low in summer or autumn. There are various possible explanations for this trend. Firstly, the anthropogenic emissions of these pollutants are increased in winter through, e.g., increased heating. Furthermore, snow cover reduces the dry deposition of trace gases. In addition, the average boundary layer height is lower during the winter, which decreases the dilution of emissions. O_3, on the other hand, had a peak in spring (April) and a low point in autumn (October). This is typical for non-urban sites in Northern Europe. In the spring, increased mixing with the free troposphere and stratosphere results in increased ozone concentrations. During summer, the ozone concentration decreases again due to substantial stomatic activity, increased dry deposition, and photochemical destruction (Ruuskanen *et al.* 2003).

Figure 9a,e shows the monthly medians of the monoterpene and isoprene concentrations above the canopy over the years 2010 to 2020. From previous work, we know that most VOCs at SMEAR II originate from biogenic sources (Heikkinen *et al.* 2020a). As expected, monoterpene and isoprene concentrations showed a peak in summer, as this coincides with the growing season of the boreal forest. There was a clear positive correlation between the ecosystem BVOC fluxes and the atmospheric VOC concentrations of isoprene and monoterpenes (Fig. 2; r = 0.92 and 0.95, respectively). In the exceptionally warm and dry years 2010 and 2018, also unusually high concentrations of isoprene and monoterpenes were measured over the summer months (Fig. 9a,e). In 2018, the maximum summer isoprene and monoterpene concentrations were 2–3 times higher than the long-term median concentrations in summer months.

H_2SO_4, the HOM monomers (m/z 290–430) and the HOM dimers (m/z 430–620) all had a concentration peak in summer (Fig. 9f–h) and minima in winter. For HOMs, the summer peak is likely linked to the increase in VOC concentrations (Fig. 9a,e) due to pronounced emissions from the vegetation. It is known that the forest ecosystem releases more VOCs during summer (Aaltonen *et al.* 2013). Those emissions from the ecosystem directly impact the atmospheric concentrations. Among the most significant biogenic VOCs at SMEAR II, isoprene and monoterpenes emissions are also impacted by meteorological factors, such as radiation and temperature, thus impacting on concentrations of their resulting oxidation products, e.g., HOMs. Besides the increase in HOM precursor concentrations at higher temperatures, (Quéléver *et al.* 2019) showed that the formation of HOM is temperature dependent and the first steps of the autoxidation leading to HOM formation is enhanced with increasing temperatures, justifying an increased HOM yield in warmer seasons. Additionally, the increase of radiation — already before summertime — could easily favour the OH-initiated oxidation pathway (as opposed to ozonolysis pathway) prior to the autoxidation reaction.

Lastly, H_2SO_4 has precursors that are formed through photochemical reactions in the atmosphere, with global radiation also peaking in summer. It is then in line with the observed H_2SO_4 maximum concentration during summertime, along with the peak of global radiation (Stone *et al.* 2012).

Links with environmental factors

The most important atmospheric oxidants for VOCs are the hydroxyl radical ($OH^{\bullet}$, or OH for short), ozone and the nitrate radical ($NO_3^{\bullet}$, or NO_3 for short). Of these oxidants, NO_3 has the largest monoterpene oxidation potential (Peräkylä *et al.* 2014; Yan *et al.* 2016). Under influence of radiation, NO_3 is, however, rapidly photolysed. Oxidation of monoterpenes with NO_3 occurs, therefore, almost exclusively at night. On the other hand, oxidation with OH only happens during the daytime, as OH formation requires UV radiation. Ozone has the capacity to oxidate VOCs during both day and night. Of the three oxidants, only ozone has been continuously measured at the SMEAR II station. To estimate the concentrations of OH and NO_3, proxies are often employed (e.g., Kontkanen *et al.* 2016). Due to its formation under influence of UV radiation, OH strongly correlates with global radiation. Global radiation can, therefore, be used as a proxy for OH. Similarly, NO_3 is formed by reactions between ozone and NO_2, making $[O_3][NO_2]$ a reasonable proxy. Here, $[NO_2]$ is obtained as the difference between the NO and NO_x concentration.

In Fig. 10, scatter plots are presented of the HOM monomer concentration as a function of $[O_3]$, global radiation, and $[O_3][NO_2]$, respectively. The HOM monomer concentration shows a clear positive correlation (r = 0.77) with global radiation (proxy for OH), a clear negative correlation (r = –0.52) with $[O_3][NO_2]$ (proxy for NO_3), and no clear correlation (r = 0.19) with $[O_3]$. Regardless of these respective correlations, (Peräkylä *et al.* 2014) indicate that NO_3 (nighttime) and O_3 (daytime) dominate the oxidation capacity of monoterpenes. Furthermore, (Jokinen *et al.* 2015) have shown that O_3 oxidation pathways produce significantly higher HOM yields than OH pathways. The correlations found here, therefore, seem to indicate that the monoterpene (or other VOC) concentration is the rate

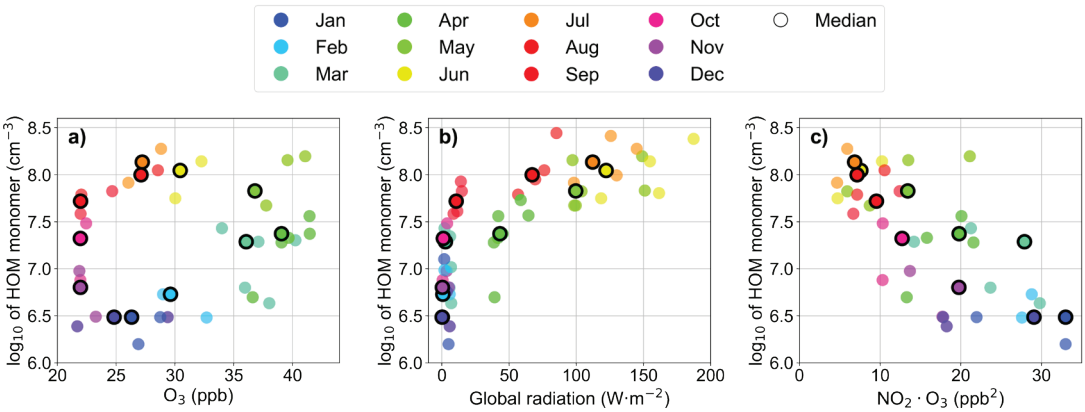

Fig. 10. $\log_{10}$ of HOM monomer vs. (**a**) O_3; (**b**) Global radiation; and (**c**) $NO_2 \cdot O_3$. Monthly medians of single years are indicated with different colours and the medians of monthly medians over all years are indicated with black outline. Data from years 2011–2020 is included.

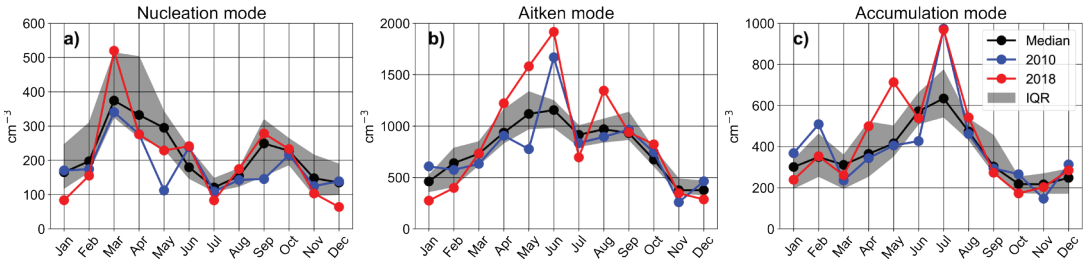

Fig. 11. Monthly medians of (**a**) nucleation; (**b**) Aitken; and (**c**) accumulation mode aerosol particle number concentrations. The medians of monthly medians over all years are shown in black with interquartile range (IQR) in grey shading. Monthly medians of years 2010 and 2018 are shown in blue and red, respectively. Data coverage of all modes is 1996–2020.

limiting factor in HOM formation rather than the concentrations of the oxidants. It is also important to note that diurnal cycles are not observable in these scatter plots. The observed correlations can be affected by this statistical restriction.

Atmospheric aerosol particle number concentrations

Monthly variation

The annual cycle of monthly atmospheric aerosol particle concentrations measured with the DMPS during period 1997–2020 are presented in Fig. 11 for nucleation (3–25 nm), Aitken (25–100 nm), and accumulation (100–1000 nm) particle modes. The monthly medians over all size classes showed distinctive seasonal variation. Nucleation mode particle concentrations peaked during spring months with lower concentrations during summer. A secondary concentration maximum was found in September. Aitken and accumulation mode particle concentrations were higher in summer, although the peak in Aitken mode particle concentrations occurred slightly earlier and was longer-lasting compared with the accumulation mode. Both years 2010 and 2018 had some notable deviations from the 1997–2020 monthly medians, with substantially higher concentrations in both Aitken and accumulation mode during summer. This can be explained by the overall higher temperatures and more global radiation during those summers (Fig. 3), leading to enhanced BVOC emissions and further to high HOM concentrations (Fig. 9), which allows the particles to grow more efficiently. In nucleation mode, high spring-time concentrations were found only in 2018. The sink from the bigger particles was

lower than the median in spring 2018, which enables a larger fraction of particles from NPF events to survive coagulation scavenging and, therefore, enables higher nucleation mode particle concentrations. Notably low nucleation mode particles concentrations were observed during the rainy May of 2010 (Fig. 3d), when a lower-than-average amount of global radiation was present, decreasing the probability of NPF (Dada *et al.* 2017).

CS and NPF events generally had contrasting seasonal cycles, with lower values of CS in months with increased NPF events and vice versa (Fig. 12). In 2018, levels of CS were higher than usual for the whole year, except in March, when the concentration of nucleation mode particles was high (Fig. 11). The high CS value of July 2018 related well to only one NPF event in that month.

Links with environmental factors

As seen in Fig. 2, the correlations between atmospheric aerosol particle number concentrations of different size classes and the various meteorological variables were rather low, especially for nucleation mode particles. Slightly stronger correlations were found for Aitken and accumulation mode particles.

Scatter plots between the modal particle concentrations and the global radiation and RH are presented in Fig. 13. These results can to a large extent be explained by the combined effects of the sources and sinks of particles in each mode. Nucleation mode particles originated almost entirely from NPF in this environment, which peaks during the spring and autumn (Fig. 12b). Nucleation mode particles are removed by their coagulation with larger particles and by their growth into the Aitken mode, both being strongest in summer due to high CS (Fig. 12a) and high particle growth rates associated with high radiation intensities and temperatures causing high concentration of condensing trace gases (Fig. 9f–h; Liao *et al.* 2014; Paasonen *et al.* 2018). Outside the winter period, the largest fraction of both Aitken and accumulation mode particles originates from the growth of lower particles sizes, and this growth may turn into a sink of Aitken mode particles at the highest temperatures. High values of RH suppress NPF (Dada *et al.* 2017; Kerminen *et al.* 2018) and tend to be associated with rain, which is usually the main sink of accumulation mode particles and a potentially important sink of both Aitken and nucleation mode particles (e.g., Zikova, 2016).

H_2SO_4 has been observed to be an essential initiator of NPF and, together with bases, such as ammonia and amines, and HOMs, is able to grow newly formed clusters into atmospheric aerosol particles (e.g., Lehtipalo *et al.* 2018, Bianchi *et al.* 2019). In Fig. 14, the sub-2-nm atmospheric aerosol particle number concentration is plotted against the H_2SO_4, HOM monomer, HOM dimer concentrations. The figures show a reasonable correlation (r = 0.47–0.61) between the number concentration of sub-2-nm atmospheric aerosol particles and the concentration of H_2SO_4 and HOMs. This is consistent with condensing trace gases contributing to the formation of these sub-2-nm particles.

Atmospheric aerosol particle mass concentration and optical properties

Monthly variation

At SMEAR II, most of the PM1 and PM2.5 aerosol particles consisted of organics (Fig. 15), reflecting the influence of the biogenic environment on the particle composition. The second-largest aerosol species was SO_4^{2-} followed by NH_4^+ and eBC. The aerosol particle chemical composition varied throughout the year as the fraction of organics increased in summer and the fraction of inorganic aerosols increased in winter (SO_4^{2-}, NO_3^-, NH_4^+, eBC) (Fig. S11 in Supplementary Information).

Following the annual cycle of VOCs, organic aerosols had a clear annual cycle with a maximum concentration of 2.5 μg m^{-3} in summer and a minimum in winter. In contrast, the highest SO_4^{2-}, NH_4^+, NO_3^-, and Cl^- concentrations occurred in winter (0.8, 0.3, 0.2, and 0.02 μg m^{-3}, respectively), with lower concentrations outside the winter season (Fig. 16b–e).

Following the total mass concentration of atmospheric aerosol species (Fig. 15), PM1,

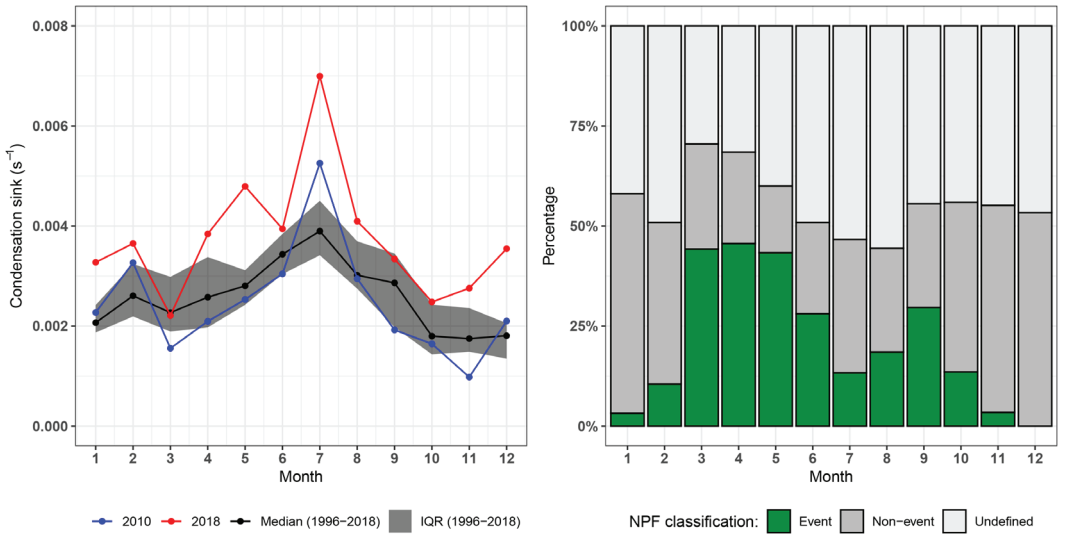

Fig. 12. (**a**) monthly median values of condensation sink and (**b**) monthly medians of proportions of days classified as new particle formation events, non-events or undefined.

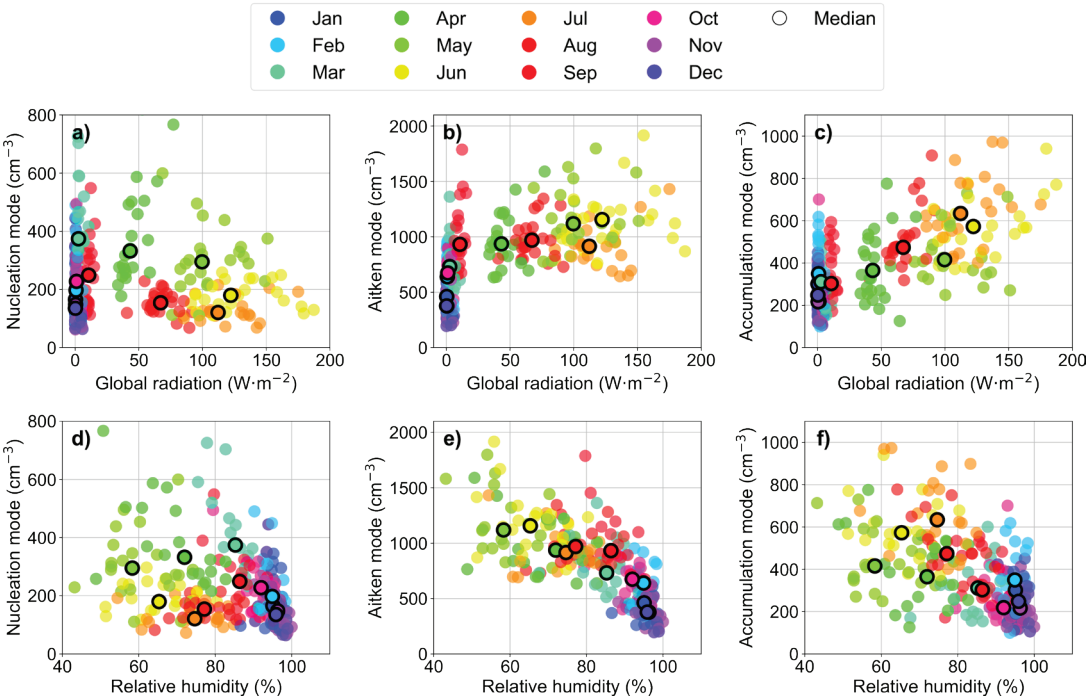

Fig. 13. Global radiation (top row) and relative humidity (bottom row) vs. nucleation (**a**,**d**); Aitken (**b**,**e**); and accumulation (**c**,**f**) mode particle number concentrations measured by DMPS instrument. Monthly medians of single years are indicated with different colours and the medians of monthly medians over all years are indicated with black outline. Data from years 1997–2020 and 1999–2020 is included in plots of global radiation and relative humidity, respectively.

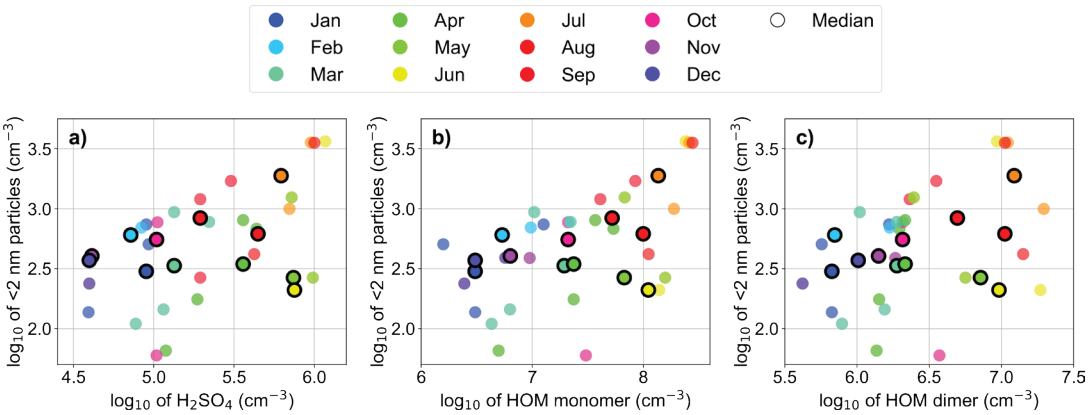

Fig. 14. $\log_{10}$ of sub-2-nm particle number concentration vs. (**a**) $\log_{10}$ of H_2SO_4; (**b**) $\log_{10}$ of HOM monomer; and (**c**) $\log_{10}$ of HOM dimer concentrations. Monthly medians of single years are indicated with different colours and the medians of monthly medians over all years are indicated with black outline. Data from years 2016–2020 is included.

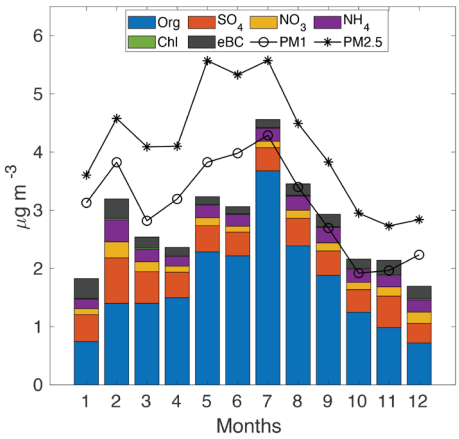

Fig. 15. Monthly medians of aerosol mass (PM1 and PM2.5; 2000–2020) and monthly medians of chemical composition (2012–2019).

PM2.5, and PM10 had the highest mass concentrations during the summer period reaching 4.3, 5.6, and 6.8 μg m^{-3}, respectively (Fig. 16f–h). In addition, in February, peaks could be detected for PM1, PM2.5, and PM10. The annual cycles of chemical composition and PM reflected in turn on aerosol optical properties (AOPs) (Fig. 16i–l). Scattering and backscattering coefficients were highest during February and summer whereas the absorption coefficient was highest in winter, specifically in February. As eBC is derived from the absorption coefficient (Petzold *et al.* 2013), eBC followed the annual cycle of absorption. The February peaks in scattering and backscattering coefficients can be explained by increased PM and accumulation mode aerosol number concentration whereas the summer peak is mainly caused by organic aerosols. Scattering, backscattering, and absorption coefficients depend also on the total volume of particles (e.g., Luoma *et al.* 2019).

Warmer than usual temperatures during the summers of 2010 and 2018 led to higher organic aerosol and PM concentrations, and, therefore, to increased scattering and backscattering coefficients. The peaks in May were also higher for PM10 (both years) as well as for PM1 and PM2.5 (year 2010) and are potentially caused by pollen (Manninen *et al.* 2014). Higher temperatures can enhance SOA production and, therefore, lead to elevated organic aerosol concentrations and PM. Long-range transport of wildfire emissions (such as black and brown carbon) can also play a role in the increased PM observed in July 2010 and 2018 as well as in increased organic concentrations and a slightly increased absorption coefficient observed in July 2018. Wildfires occurred in July and August in Russia in 2010 (Corrigan *et al.* 2013) and in Sweden in 2018 (Krikken *et al.* 2019).

Links with environmental factors

As previous studies have suggested (e.g., Williams *et al.* 2011, Heikkinen *et al.* 2020b, Yli-Juuti *et al.*

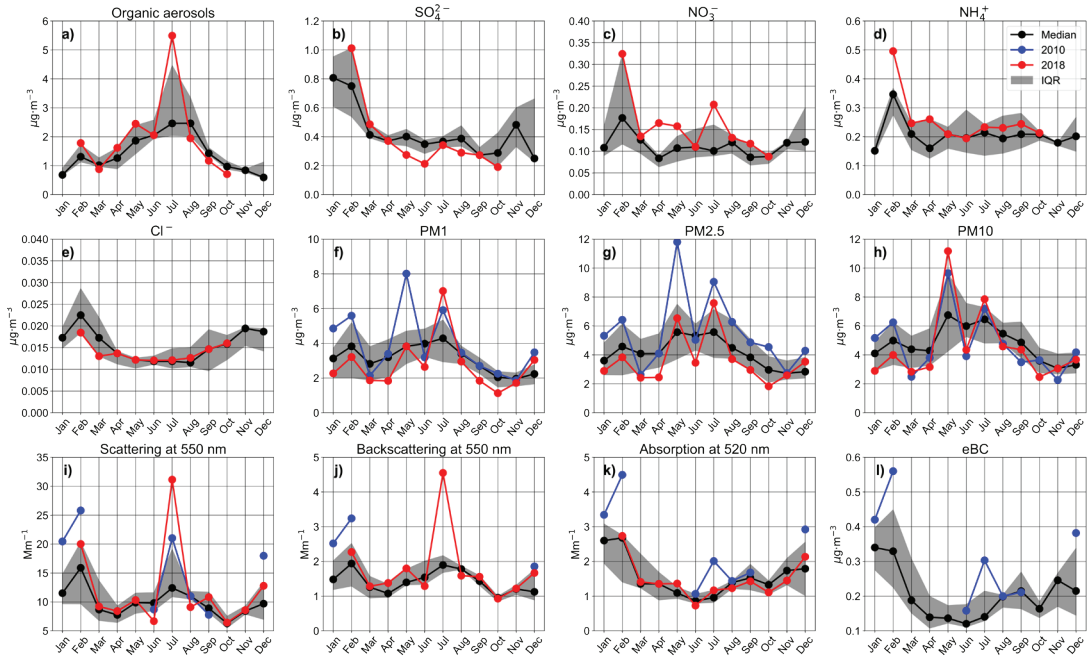

Fig. 16. Monthly medians of (**a**) organics; (**b**) sulphate (SO_4^{2-}); (**c**) nitrate (NO_3); (**d**) ammonium (NH_4^+); (**e**) chloride (Cl^-); (**f**) PM1; (**g**) PM2.5; (**h**) PM10; (**i**) scattering coefficient at 550 nm; (**j**) backscattering coefficient at 550 nm; (**k**) absorption coefficient at 520 nm; and (**l**) equivalent black carbon concentration (eBC). The medians of monthly medians over all years are shown in black with interquartile range (IQR) in grey shading. Monthly medians of years 2010 and 2018 are shown in blue and red, respectively. Atmospheric aerosol particle chemical composition data covers 2012–2019, while atmospheric aerosol particle chemical composition covers 2000–2021.

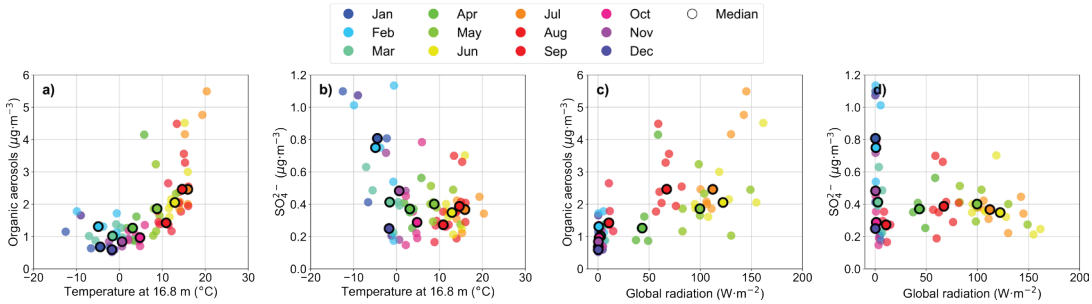

Fig. 17. Organics and sulphate (SO_4^{2-}) vs. air temperature at 16.8 m (**a**,**b**) and global radiation (**c**,**d**). Monthly medians of single years are indicated with different colours and the medians of monthly medians over all years are indicated with black outline. Data from years 2000–2020 is included.

2021), we find that increased temperature and radiation increased the organic aerosol concentration (r = 0.65 and 0.66, respectively) (Fig. 17a,c), in line with the emissions of VOCs themselves. Figure 17b,d shows that colder temperatures and suppressed radiation led to increased SO_4^{2-} concentrations in winter (r = –0.30 and –0.25, respectively). The influence of the air mass origin can be seen in Fig. S12 in Supplementary Information: the highest inorganic aerosol concentrations can be associated with air masses transported from Europe and Russia, especially in winter. SO_4^{2-} arrived in SMEAR II mainly from Russia whereas the Cl^- source area was from Europe.

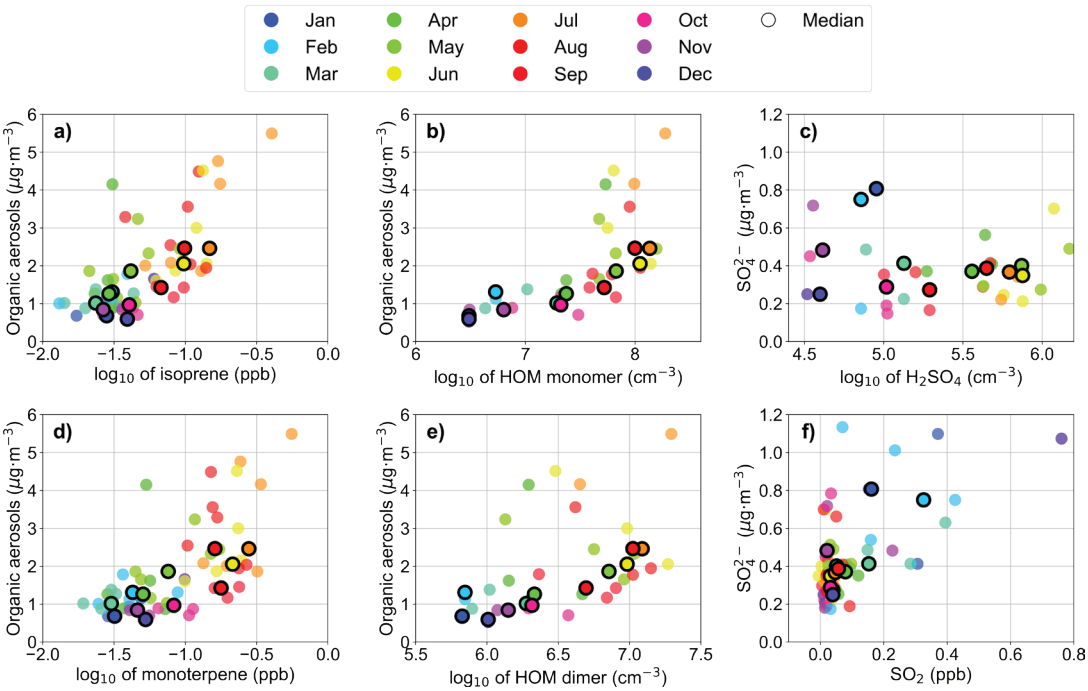

Fig. 18. Organic aerosol concentration vs. $\log_{10}$ of (**a**) isoprene; (**b**) HOM monomer; (**d**) monoterpene; and (**e**) HOM dimer concentrations, as well as sulphate (SO_4^{2-}) vs. $\log_{10}$ of (**c**) H_2SO_4 and (**f**) SO_2 concentrations. Monthly medians of single years are indicated with different colours and the medians of monthly medians over all years are indicated with black outline. Data from years 2012–2020 is included.

Figure 18 indicates that organic aerosol concentration correlated also with isoprene and monoterpene concentrations (r = 0.71 and 0.65, respectively). Similarly, HOM monomers and dimers increased the organic aerosol concentration (r = 0.67 and non-significant 0.36, respectively), since HOMs are known to condense onto aerosols due to their low volatility. SO_4^{2-} is produced by oxidation of sulphur dioxide (SO_2), and SO_2 forms H_2SO_4. Indeed, we can see that an increase in SO_2 concentrations increased the SO_4^{2-} loading (r = 0.44).

Aerosol chemical composition affected PM and AOPs. Greater organic aerosol concentration in summer correlated with increased PM1 (r = 0.56) as well as with increased scattering and backscattering coefficients (r = 0.62 and 0.74, respectively; Fig. 19). The increase in the organic aerosol concentration in summer leads to an overall increase in atmospheric aerosol particle mass concentration, which in turn results in higher scattering and backscattering. The higher absorption coefficient in winter was due to increased concentration of black carbon. Correlations between the non-absorbing inorganic aerosol species (SO_4^{2-}, NO_3^-, and NH_4^+) and the absorption coefficient (r = 0.66, 0.61, 0.49, respectively) are likely due to the similarities between their seasonal cycles and the seasonal cycle of eBC, which is derived from the absorption coefficient. Fig. 2 indicates that SO_4^{2-}, NO_3^-, NH_4^+, and eBC were transported to SMEAR II with the same air masses (Figs. S13 and S14 in Supplementary Information) and they originated from similar sources, which in this case are likely anthropogenic. In winter, all aerosol species (excluding Cl^-) correlated well with PM1 (r = 0.33–0.86) and backscattering (r = 0.60–0.87). High scattering and backscattering occurred in winter when boundary layer height was shallow (r = –0.56 and –0.55) and when the air mass was coming from Russia (Figs. S13 and S14 in Supplementary Information). Cold winter temperatures and warm

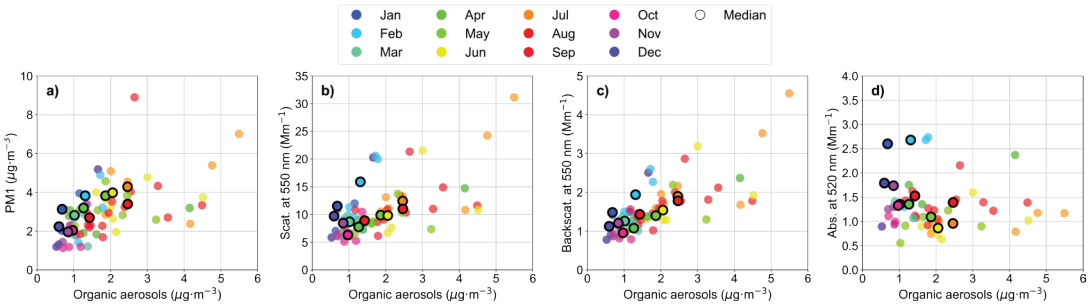

Fig. 19. Monthly medians of organic aerosols vs. (**a**) PM1; (**b**) scattering coefficient at 550 nm; (**c**) backscattering coefficient at 550 nm; and (**d**) absorption coefficient at 520 nm. Monthly medians of single years are indicated with different colours and the monthly medians over all years calculated over the whole measurement period are indicated with black outline. Data from years 2012–2020 is included.

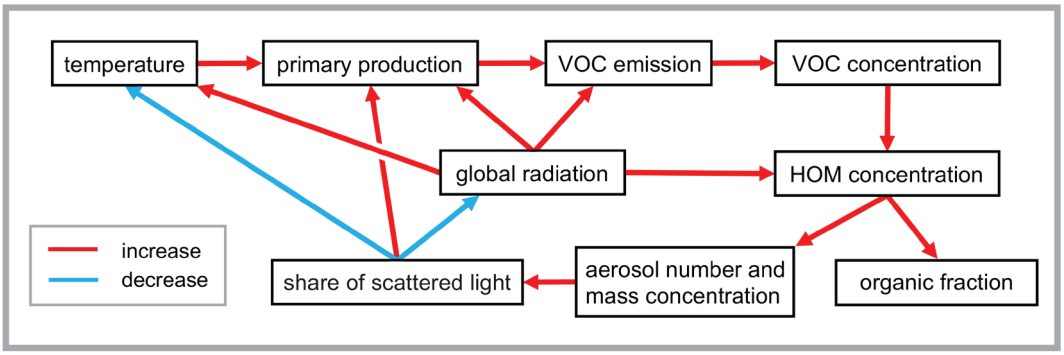

Fig. 20. Overview of relations between ecosystem and atmospheric variables. VOC: volatile organic compound, HOM: highly oxygenated organic molecule, PM: particulate mass.

summer temperatures increased scattering and backscattering coefficients (r = –0.67 and –0.63 in winter and r = 0.54 and –0.62 in summer; Fig. S13 in Supplementary Information). In winter, low temperatures indicated low boundary layer height, which explains the high scattering and backscattering coefficients. In summer, however, the positive correlation between the scattering coefficient and temperature indicates that the increased aerosol mass concentration leads to an increase in aerosol light scattering.

Summary and Conclusion

The boreal forest ecosystem and atmosphere form a strongly interconnected system, influencing each other through a myriad of complex interactions. Correlations in the seasonality between meteorological, ecosystem, and atmospheric variables can reveal these interactions. In this study, we analysed seasonal variations in the ecosystem and atmospheric data collected at the SMEAR II station, located in a boreal Scots pine forest, between 1996 and 2020. We additionally put focus on the years 2010 and 2018, that had extraordinary warm and dry summers, to study the effects of these exceptional climate events on the boreal forest ecosystem-atmosphere interactions.

Most studied variables of the boreal forest ecosystem-atmosphere system showed clear seasonality, along with significant correlations between the variables. With the increase in global radiation in spring, together with the resulting increase in air and soil temperature, the plant growth season is initiated. Both the gross primary production (GPP), uptake of carbon by the ecosystem, and the ecosystem respiration (RE), emission of carbon by the ecosystem, intensify

during this active season, with a peak in summer. In late spring to early summer, the GPP is larger than the RE, making the boreal forest a carbon sink. Besides carbon dioxide, the ecosystem also releases volatile organic compounds (VOC), such as isoprene and monoterpene. Following the increased plant activity, the VOC emissions also peak in summer, specifically at ecosystem scale.

Once in the atmosphere, VOCs can be oxidised, through many complex reaction pathways, to form highly oxygenated organic molecules (HOMs). Although the exact interactions between variables leading to increased HOM formation is difficult to map out, it is presumable that increases in global radiation, air temperature, and VOC concentration boost HOM formation. Alongside global radiation, air temperature and VOC concentration, HOM formation has its peak in summer.

HOMs have been proposed to play a role in stabilising molecular clusters and in growing them into larger-size atmospheric aerosol particles. We indeed see significant correlations between the seasonal variation in the HOM concentration and the number and mass concentrations of atmospheric aerosol particles. HOMs have their highest concentration in summer, likely leading to increased condensation onto existing atmospheric aerosol particles. The result is high number concentrations of Aitken and accumulation mode particles in late spring and summer.

The increased VOC emissions by the ecosystem in summer, and the related high atmospheric concentrations of HOMs, not only affect the concentration of atmospheric aerosol particles, but also their composition. The contribution of organic compounds to the atmospheric aerosol particle composition is highest in summer, following the peak in VOC and HOM concentrations. Atmospheric aerosol particles scatter solar radiation. The peak of Aitken and accumulation mode particles in summer will thus result in increased scattering of solar radiation.

Of the studied period, the years 2010 and 2018 had the highest air temperatures in summer, accompanied by relative dryness. Our results indicate that the boreal forest ecosystem around the SMEAR II station can cope with the additional stress of these warm and dry summers. Rather than halting plant growth, the GPP was largely higher in the summer of these years, leading to an increased carbon sink in the studied temperature-limited boreal forest ecosystem.

The ability of the ecosystem to not only cope, but also increase GPP, with the increased air temperature and dryness, results in higher emissions of VOCs. With higher temperatures, global radiation, and VOC concentrations, the concentration of HOMs is also elevated.

The concentration of atmospheric aerosol particles in the different size ranges depends on a variety of factors. An increase of condensing trace gases, such as sulfuric acid and HOMs, generally leads to larger concentrations of aerosol particles in the larger size ranges. This can, however, be offset by precipitation, a major sink for atmospheric aerosol particles. Additionally, the concentration of atmospheric aerosol particles of smaller sizes can be decreased through enhanced growth into larger sizes. Generally, warm, and dry summers (specifically as seen in 2018), result in increased number and mass concentrations of atmospheric aerosol particles. Furthermore, the increased VOC emissions from the ecosystem give rise to a larger fraction of organics in the atmospheric aerosol particles. The increased concentration of atmospheric aerosol particles leads to heightened scattering of solar radiation.

Our study provides field evidence of a negative feedback loop, where higher global radiation leads indirectly to increased scattering of radiation, through increased emissions of organics from the ecosystem, which undergo oxidation reactions and subsequently condense onto radiation scattering atmospheric aerosol particles. Atmospheric aerosol particles scatter radiation both directly, and indirectly, by functioning as nuclei for cloud condensation. This scattering has a net cooling effect on the climate. Additionally, the ecosystem relies on radiation for its growth, but trees can use scattered radiation more efficiently than direct radiation. Scattering of solar radiation thus increases the ecosystem growth, which again further enhances emission of organics. This feedback loop is illustrated in Fig. 20.

Climate change is expected to increase the occurrence of warm summers and the likelihood and intensity of dry summer periods in

Northern Europe (Ruosteenoja *et al.* 2018). This study highlights the reaction of a boreal forest to warmer and drier than usual summer conditions. The continuous measurements of meteorological, ecosystem and atmospheric variables together in the same location for over two and half decades, as done at the SMEAR II station, is unique. Comprehensive, long-term measurements are crucial to study the complex interactions between ecosystem and atmosphere, and responses and feedbacks to climate (Kulmala *et al.* 2004, 2014, 2020). Future studies could focus on the limits of the increase in primary production during warm summers. Heat, coupled with dry conditions, should eventually negatively impact the primary production. Furthermore, as ozone concentration and new particle formation events peak in spring, exceptionally warm springs and autumns could provide further interesting avenues for research. In this study, we have mostly focused on direct scattering by atmospheric aerosol particles and have not investigated the complex interactions between atmospheric aerosol particle properties and cloud properties. Changes in atmospheric aerosol particle precursor emissions and concentrations can, for instance, significantly affect cloud properties, such as the reflectivity (Petäjä *et al.* 2021). As there are currently no long-term observations available of aerosol-cloud interactions, this should be integrated in future long-term studies.

Acknowledgements: We acknowledge the following projects and funding sources: ACCC Flagship funded by the Academy of Finland grant number 337549, Academy professorship funded by the Academy of Finland (grant no. 302958), Academy of Finland projects no. 1325656, 316114 and 325647, "Quantifying carbon sink, CarbonSink+ and their interaction with air quality" project funded by Jane and Aatos Erkko Foundation, European Research Council (ERC) project ATM-GTP Contract No. 742206, the University of Helsinki Three Years Research Grant, and the Maj and Tor Nessling Foundation. ICOS RI, ACTRIS RI and eLTER RI are gratefully acknowledged for the integrated long-term measurements data set at SMEAR II. We thank the technical and scientific staff in Hyytiälä for their work in maintaining the long-term measurements.

Supplementary Information: The supplementary information related to this article is available online at: http://www.borenv.net/BER/archive/pdfs/ber27/ber27-001-031-supplement.pdf

References

Aalto, J., Kolari, P., Hari, P., Kerminen, V.-M., Schiestl-Aalto, P., Aaltonen, H., Levula, J., Siivola, E., Kulmala, M., & Bäck, J. (2014). New foliage growth is a significant, unaccounted source for volatiles in boreal evergreen forests. Biogeosciences, 11(5), 1331–1344.

Aalto, J., Porcar-Castell, A., Atherton, J., Kolari, P., Pohja, T., Hari, P., Nikinmaa, E., Petäjä, T., & Bäck, J. (2015). Onset of photosynthesis in spring speeds up monoterpene synthesis and leads to emission bursts. Plant, Cell & Environment, 38(11), 2299–2312.

Aalto, P., Hämeri, K., Becker, E., Weber, R., Salm, J., Mäkelä, J. M., Hoell, C., O'dowd, C. D., Hansson, H.-C., … Kulmala, M. (2001). Physical characterization of aerosol particles during nucleation events. Tellus B: Chemical and Physical Meteorology, 53(4), 344–358.

Aaltonen, H., Aalto, J., Kolari, P., Pihlatie, M., Pumpanen, J., Kulmala, M., Nikinmaa, E., Vesala, T., & Bäck, J. (2013). Continuous VOC flux measurements on boreal forest floor. Plant and Soil, 369(1), 241–256.

Aaltonen, H., Pumpanen, J., Hakola, H., Vesala, T., Rasmus, S., & Bäck, J. (2012). Snowpack concentrations and estimated fluxes of volatile organic compounds in a boreal forest. Biogeosciences, 9(6), 2033–2044.

Aaltonen, H., Pumpanen, J., Pihlatie, M., Hakola, H., Hellén, H., Kulmala, L., Vesala, T., & Bäck, J. (2011). Boreal pine forest floor biogenic volatile organic compound emissions peak in early summer and autumn. Agricultural and Forest Meteorology, 151(6), 682–691.

Alduchov, O. A., & Eskridge, R. E. (1996). Improved Magnus form approximation of saturation vapor pressure. Journal of Applied Meteorology and Climatology, 35(4), 601–609.

Baldocchi, D., Chua, H., & Reichstein, M. (2018). Interannual variability of net and gross ecosystem carbon fluxes: A review. Agricultural and Forest Meteorology, 249, 520–533.

Bianchi, F., Kurtén, T., Riva, M., Mohr, C., Rissanen, M. P., Roldin, P., Berndt, T., Crounse, J. D., Wennberg, P. O., … Ehn, M. (2019). Highly oxygenated organic molecules (HOM) from gas-phase autoxidation involving peroxy radicals: A key contributor to atmospheric aerosol. Chemical Reviews, 119(6), 3472–3509.

Bonn, B., Magh, R., Rombach, J., J, & Kreuzwieser. (2019). Biogenic isoprenoid emissions under drought stress: Different responses for isoprene and terpenes. Biogeosciences, 16, 4627–4645.

Corrigan, A., Russell, L., Takahama, S., Äijälä, M., Ehn, M., Junninen, H., Rinne, J., Petäjä, T., Kulmala, M., … Williams, J. (2013). Biogenic and biomass burning organic aerosol in a boreal forest at Hyytiälä, Finland, during HUMPPA-COPEC 2010. Atmospheric Chemistry and Physics, 13, 12233–12256.

Dada, L., Paasonen, P., Nieminen, T., Buenrostro Mazon, S., Kontkanen, J., Peräkylä, O., Lehtipalo, K., Hussein, T., Petäjä, T., … Kulmala, M. (2017). Long-term analysis of clear-sky new particle formation events and nonevents in Hyytiälä. Atmospheric Chemistry and Physics, 17(10),

6227–6241.

Dal Maso, M., Kulmala, M., Riipinen, I., Wagner, R., Hussein, T., Aalto, P., & Lehtinen, K. (2005). Formation and growth of fresh atmospheric aerosols: Eight years of aerosol size distribution data from SMEAR II, Hyytiälä, Finland. Boreal Environment Research, 10(5), 323–336.

de Gouw, J., & Warneke, C. (2007). Measurements of volatile organic compounds in the earth's atmosphere using proton-transfer-reaction mass spectrometry. Mass Spectrometry Reviews, 26(2), 223–257.

Ehn, M., Kleist, E., Junninen, H., Petäjä, T., Lönn, G., Schobesberger, S., Dal Maso, M., Trimborn, A., Kulmala, M., … Mentel, T. F. (2012). Gas phase formation of extremely oxidized pinene reaction products in chamber and ambient air. Atmospheric Chemistry and Physics, 12(11), 5113–5127.

Ehn, M., Thornton, J., Kleist, E., Sipilä, M., Junninen, H., Pullinen, I., Springer, M., Rubach, F., Tillmann, R., … Mentel, T. F. (2014). A large source of low-volatility secondary organic aerosol. Nature, 506, 476–479.

FAO. (2020). Global forest resources assessment 2020 – key findings. FAO.

Gordon, H., Kirkby, J., Baltensperger, U., Bianchi, F., Breitenlechner, M., Curtius, J., Dias, A., Dommen, J., Donahue, N. M., … Carslaw, K. S. (2017). Causes and importance of new particle formation in the present-day and preindustrial atmospheres. J. Geophys. Res.: Atmospheres, 122(16), 8739–8760.

Gray, D. W., Goldstein, A. H., & Lerdau, M. T. (2006). Thermal history regulates methylbutenol basal emission rate in Pinus ponderosa. Plant, Cell & Environment, 29(7), 1298–1308.

Grossiord, C., Buckley, T. N., Cernusak, L. A., Novick, K. A., Poulter, B., Siegwolf, R. T. W., Sperry, J. S., & McDowell, N. G. (2020). Plant responses to rising vapor pressure deficit. New Phytologist, 226(6), 1550–1566.

Guenther, A., Hewitt, C. N., Erickson, D., Fall, R., Geron, C., Graedel, T., Harley, P., Klinger, L., Lerdau, M., … Zimmerman, P. (1995). A global model of natural volatile organic compound emissions. Journal of Geophysical Research, 100(D5), 8873–8892.

Guenther, A., Jiang, X., Heald, C. L., Sakulyanontvittaya, T., Duhl, T., Emmons, L., & Wang, X. (2012). The model of emissions of gases and aerosols from nature version 2.1 (MEGAN2.1): An extended and updated framework for modeling biogenic emissions. Geosci. Model Dev., 5, 1471–1492.

Guenther, A. (2013). Biological and chemical diversity of biogenic volatile organic emissions into the atmosphere. ISRN Atmospheric Sciences, 2013, 1–27.

Hakola, H., Hellén, H., Hemmilä, M., Rinne, J., & Kulmala, M. (2012). In situ measurements of volatile organic compounds in a boreal forest. Atmos. Chem. Phys., 12, 11665–11678.

Hakola, H., Tarvainen, V., Bäck, J., Ranta, H., Bonn, B., Rinne, J., & Kulmala, M. (2006). Seasonal variation of mono- and sesquiterpene emission rates of Scots pine. Biogeosciences, 3, 93–101.

Hakola, H., Tarvainen, V., Praplan, A. P., Jaars, K., Hemmilä, M., Kulmala, M., Bäck, J., & Hellén, H. (2017). Terpenoid and carbonyl emissions from Norway spruce in Finland during the growing season. Atmos. Chem. Phys., 17, 3357–3370.

Hari, P., Kerminen, V.-M., Kulmala, L., Kulmala, M., Noe, S., Petäjä, T., Vanhatalo, A., & Bäck, J. (2017). Annual cycle of scots pine photosynthesis. Atmospheric Chemistry and Physics, 17(24), 15045–15053.

Hari, P., & Kulmala, M. (2005). Station for Measuring Ecosystem-Atmosphere Relations (SMEAR II). Boreal Environment Research, 10(5), 315–322.

Hari, P., Noe, S., Dengel, S., Elbers, J., Gielen, B., Kerminen, V., Kruijt, B., Kulmala, L., Lindroth, A., … Bäck, J. (2018). Prediction of photosynthesis in scots pine ecosystems across europe by a needle-level theory. Atmospheric Chemistry and Physics, 18(18), 13321–13328.

Heikkinen, L., Äijälä, M., Dällenbach, K., Chen, G., Garmash, O., Aliaga, D., Graeffe, F., Räty, M., Luoma, K., … Ehn, M. (2020a). Eight years of sub-micrometre organic aerosol composition data from the boreal forest characterized using a machine-learning approach [In review]. Atmospheric Chemistry and Physics.

Heikkinen, L., Äijälä, M., Riva, M., Luoma, K., Dällenbach, K., Aalto, J., Aliaga, D., Aurela, M., Keskinen, H., … Ehn, M. (2020b). Long-term sub-micrometer aerosol chemical composition in the boreal forest: Inter- and intra-annual variability. Atmospheric Chemistry and Physics, 20, 3151–3180.

Hellén, H., Hakola, H., Pystynen, K., Rinne, J., & Haapanala, S. (2006). C2-C10 hydrocarbon emissions from a boreal wetland and forest floor. Biogeosciences, 3, 167–174.

Hersbach, H., Bell, B., Berrisford, P., Hirahara, S., Horányi, A., Muñoz-Sabater, J., Nicolas, J., Peubey, C., Radu, R., … Thépaut, J.-N. (2020). The ERA5 global reanalysis. Quarterly Journal of the Royal Meteorological Society, 146, 1999–2049.

IPCC. (2021). IPCC, 2021: Climate change 2021: The physical science basis. contribution of working group I to the sixth assessment report of the intergovernmental panel on climate change (V. Masson-Delmotte, P. Zhai, A. Pirani, S. Connors, C. Péan, S. Berger, N. Caud, Y. Chen, L. Goldfarb, … B. Zhou, Eds.). Cambridge University Press.

Janson, R. W. (1993). Monoterpene emissions from Scots pine and Norwegian spruce. J Geophys Res, 98, 2839–2850.

Jokinen, T., Sipilä, M., Junninen, H., Ehn, M., Lönn, G., Hakala, J., Petäjä, T., Mauldin III, R. L., Kulmala, M., & Worsnop, D. R. (2012). Atmospheric sulphuric acid and neutral cluster measurements using CI-APi-TOF. Atmospheric Chemistry and Physics, 12(9), 4117–4125.

Jokinen, T., Berndt, T., Makkonen, R., Kerminen, V.-M., Junninen, H., Paasonen, P., Stratmann, F., Herrmann, H., Guenther, A. B., … Sipilä, M. (2015). Production of extremely low volatile organic compounds from biogenic emissions: Measured yields and atmospheric implications. Proceedings of the National Academy of Sciences, 112(23), 7123–7128.

Junninen, H., Ehn, M., Petäjä, T., Luosujärvi, L., Kotiaho, T., Kostiainen, R., Rohner, U., Gonin, M., Fuhrer, K., … Worsnop, D. R. (2010). A high-resolution mass

spectrometer to measure atmospheric ion composition. Atmospheric Measurement Techniques, 3(4), 1039–1053.

Junninen, H., Lauri, A., Keronen, P., Aalto, P., Hiltunen, V., Hari, P., & Kulmala, M. (2009). Smart-SMEAR: On-line data exploration and visualization tool for SMEAR stations. Boreal Environment Research.

Kellomäki, S., Strandman, H., Heinonen, T., Asikainen, A., Venäläinen, A., & Peltola, H. (2018). Temporal and spatial change in diameter growth of boreal Scots pine, Norway spruce, and birch under recent-generation (cmip5) global climate model projections for the 21st century. Forests, 9(3).

Kerminen, V.-M., Chen, X., Vakkari, V., Petäjä, T., Kulmala, M., & Bianchi, F. (2018). Atmospheric new particle formation and growth: Review of field observations. Environ. Res. Lett., 13(10).

Keskinen, H., Kesti, J., Aalto, P., Levula, J., Kulmala, M., & Petäjä, T. (2016). Aerosol mass concentration measurements at smearii. In A. Lintunen, J. Enroth, S. Häme, & M. Kulmala (Eds.), Proceedings of 'the centre of excellence in atmospheric science (coe atm) – from molecular and biological processes to the global climate' annual meeting 2016. Finnish Association for Aerosol Research.

Keskinen, H.-M., Ylivinkka, I., Heikkinen, L., Aalto, P., Nieminen, T., Lehtipalo, K., Aalto, J., Levula, J., Kesti, J., … Petäjä, T. (2020). Long-term aerosol mass concentrations in southern Finland: Instrument validation, seasonal variation and trends. Atmospheric Measurement Techniques, in review.

Kolari, P., Bäck, J., Taipale, R., Ruuskanen, T. M., Kajos, M. K., Rinne, J., Kulmala, M., & Hari, P. (2012). Evaluation of accuracy in measurements of voc emissions with dynamic chamber system. Atmospheric Environment, 62, 344–351.

Kontkanen, J., Paasonen, P., Aalto, J., Bäck, J., Rantala, P., Petäjä, T., & Kulmala, M. (2016). Simple proxies for estimating the concentrations of monoterpenes and their oxidation products at a boreal forest site. Atmospheric Chemistry and Physics, 16(20), 13291–13307.

Krikken, F., Lehner, F., Haustein, K., Drobyshev, I., & van Oldenborgh, G. J. (2019). Attribution of the role of climate change in the forest fires in Sweden 2018. Nat. Hazards Earth Syst. Sci. Discuss., in review.

Kulmala, L., Pumpanen, J., Kolari, P., Dengel, S., Berninger, F., Köster, K., Matkala, L., Vanhatalo, A., Vesala, T., & Bäck, J. (2019). Inter- and intra-annual dynamics of photosynthesis differ between forest floor vegetation and tree canopy in a subarctic scots pine stand. Agricultural and Forest Meteorology, 271, 1–11.

Kulmala, M., Ezhova, E., Kalliokoski, T., Noe, S., Vesala, T., Lohila, A., Liski, J., Makkonen, R., Bäck, J., … Kerminen, V.-M. (2020). Carbonsink+: Accounting for multiple climate feedbacks from forests. Boreal Environment Research, 25, 145–159.

Kulmala, M., Nieminen, T., Nikandrova, A., Lehtipalo, K., Manninen, H. E., Kajos, M. K., Kolari, P., Lauri, A., Petäjä, T., … V.-M., K. (2014). CO_2 -induced terrestrial climate feedback mechanism: From carbon sink to aerosol source and back. Boreal Environment Research, 19 (suppl. B), 122–131.

Kulmala, M., Suni, T., Lehtinen, K. E. J., Dal Maso, M., Boy, M., Reissell, A., Rannik, Ü., Aalto, P., Keronen, P., … Hari, P. (2004). A new feedback mechanism linking forests, aerosols, and climate. Atmospheric Chemistry and Physics, 4(2), 557–562.

Kulmala, M., Lintunen, A., Ylivinkka, I., Mukkala, J., Rantanen, R., Kujansuu, J., Petäjä, T., & Lappalainen, H. K. (2021). Atmospheric and ecosystem big data providing key contributions in reaching united nations' sustainable development goals. Big Earth Data, 5(3), 277–305.

Kulmala, M., Petäjä, T., Nieminen, T., Sipila, M., Manninen, H. E., Lehtipalo, K., Dal Maso, M., Aalto, P. P., Junninen, H., … Kerminen, V.-M. (2012). Measurement of the nucleation of atmospheric aerosolparticles. Nature Protocols, 7, 1651–1667.

Kurtén, T., Kulmala, M., Maso, M. D., Suni, T., Reissell, A., Vehkamäki, H., Hari, P., Laaksonen, A., Viisanen, Y., & Vesala, T. (2003). Estimation of different forest-related contributions to the radiative balance using observations in southern Finland. Boreal Environ. Res., 8, 275–485.

Launiainen, S. (2010). Seasonal and inter-annual variability of energy exchange above a boreal Scots pine forest. Biogeosciences, 7(12), 3921–3940.

Lehtipalo, K., Yan, C., Dada, L., Bianchi, F., Xiao, M., Wagner, R., Stolzenburg, D., Ahonen, L. R., Amorim, A., … Worsnop, D. R. (2018). Multicomponent new particle formation from sulfuric acid, ammonia, and biogenic vapors. Science Advances, 4(12).

Liao, L., Kerminen, V.-M., Boy, M., Kulmala, M., & Dal Maso, M. (2014). Temperature influence on the natural aerosol budget over boreal forests. Atmospheric Chemistry and Physics, 14(16), 8295–8308.

Lihavainen, H., Asmi, E., Aaltonen, V., Makkonen, U., & Kerminen, V.-M. (2015). Direct radiative feedback due to biogenic secondary organic aerosol estimated from boreal forest site observations. Environmental Research Letters, 10(10), 104005.

Lihavainen, H., Kerminen, V.-M., Tunved, P., Aaltonen, V., Arola, A., Hatakka, J., Hyvärinen, A., & Viisanen, Y. (2009). Observational signature of the direct radiative effect by natural boreal forest aerosols and its relation to the corresponding first indirect effect. Journal of Geophysical Research: Atmospheres, 114(D20).

Loreto, F., & Schnitzler, J. (2010). Abiotic stresses and induced BVOCs. Trends in Plant Science, 15(3), 154–166.

Luoma, K., Virkkula, A., Aalto, A., Petäjä, P., & Kulmala, M. (2019). Over a 10-year record of aerosol optical properties at SMEAR II. Atmospheric Chemistry and Physics, 19, 11363–11382.

Mäki, M., Aalto, J., Hellén, H., Pihlatie, M., & Bäck, J. (2019a). Interannual and seasonal dynamics of volatile organic compound fluxes from the boreal forest floor. Front Plant Sci, 10, 191.

Mäki, M., Aaltonen, H., Heinonsalo, J., Hellén, H., Pumpanen, J., & Bäck, J. (2019b). Boreal forest soil is a significant and diverse source of volatile organic compounds. Plant and Soil, 441(1), 89–110.

Mäki, M., Heinonsalo, J., Hellén, H., & Bäck, J. (2017). Contribution of understorey vegetation and soil processes to boreal forest isoprenoid exchange. Biogeosciences, 14(5), 1055–1073.

Manninen, A. J., Marke, T., Tuononen, M., & O'Connor, E. J. (2018). Atmospheric boundary layer classification with doppler lidar. Journal of Geophysical Research: Atmospheres, 123(15), 8172–8189.

Manninen, H., Back, J., Sihto-Nissila, S.-L., Huffman, J., Pessi, A.-M., Hiltunen, V., Aalto, P., Hidalgo, P., Hari, P., … Petaja, T. (2014). Patterns in airborne pollen and other primary biological aerosol particles (pbap), and their contribution to aerosol mass and number in a boreal forest. Boreal Environment Research, 19(suppl. B), 383–405.

Monteith, J. L., & Unsworth, M. H. (2014). Principles of environmental physics (4th edn). Academic Press.

Mutzel, A., Poulain, L., Berndt, T., Iinuma, Y., Rodigast, M., Böge, O., Richters, S., Spindler, G., Sipilä, M., … Herrmann, H. (2015). Highly oxidized multifunctional organic compounds observed in tropospheric particles: A field and laboratory study. Environ. Sci. Technol., 49, 7754–7761.

Nadal-Sala, D., Grote, R., Birami, B., Lintunen, A., Mammarella, I., Preisler, Y., Rotenberg, E., Salmon, Y., Tatarinov, F., … Ruehr, N. K. (2021). Assessing model performance via the most limiting environmental driver in two differently stressed pine stands. Ecological Applications, e02312.

Nieminen, T., Asmi, A., Dal Maso, M., Aalto, P. P., Keronen, P., Petäjä, T., Kulmala, M., & Kerminen, V.-M. (2014). Trends in atmospheric new-particle formation: 16 years of observations in a boreal-forest environment. Boreal Environment Research, 19, 191–214.

Niinemets, Ü., Loreto, F., & Reichstein, M. (2004). Physiological and physicochemical controls on foliar volatile organic compound emissions. Trends in Plant Science, 9(4), 180–186.

Paasonen, P., Peltola, M., Kontkanen, J., Junninen, H., Kerminen, V.-M., & Kulmala, M. (2018). Comprehensive analysis of particle growth rates from nucleation mode to cloud condensation nuclei in boreal forest. Atmospheric Chemistry and Physics, 18(16), 12085–12103.

Paasonen, P., Asmi, A., Petäjä, T., Kajos, M. K., Äijälä, M., Junninen, H., Holst, T., Abbatt, J. P. D., Arneth, A., … Kulmala, M. (2013). Warming-induced increase in aerosol number concentration likely to moderate climate change. Nat. Geosci., 6, 438–442.

Paramonov, M., Aalto, P. P., Asmi, A., Prisle, N., Kerminen, V. M., Kulmala, M., & Petäjä, T. (2013). The analysis of size-segregated cloud condensation nuclei counter (CNC) data and its implications for aerosol-cloud interactions. Atmos. Chem. Phys., 13, 10285–10301.

Peng, C., Ma, Z., Lei, X., Zhu, Q., Chen, H., Wang, W., Liu, S., Li, W., Fang, X., & Zhou, X. (2012). A drought-induced pervasive increase in tree mortality across Canada's boreal forests. Nature Climate Change volume, 1(9), 467–471.

Peräkylä, O., Vogt, M., Tikkanen, O., Laurila, T., Kajos, M., Rantala, P., Patokoski, J., Aalto, J., Yli-Juuti, T., Ehn, M. *et al.* (2014). Monoterpenes' oxidation capacity and rate over a boreal forest: Temporal variation and connection to growth of newly formed particles. Boreal Environment Research, 19(Suppl. B), 293–310.

Petäjä, T., Tabakova, K., Manninen, A., Ezhova, E., O'Connor, E., Moisseev, D., Sinclair, V. A., Backman, J., Levula, J., … Kerminen, V.-M. (2021). Influence of biogenic emissions from boreal forests on aerosol–cloud interactions. Nature Geoscience, 15, 42–47.

Petzold, A., Ogren, J. A., Fiebig, M., Laj, P., Li, S.-M., Baltensperger, U., Holzer-Popp, T., Kinne, S., Pappalardo, G., … Zhang, X.-Y. (2013). Recommendations for reporting "black carbon" measurements. Atmospheric Chemistry and Physics, 13(16), 8365–8379.

Piao, S., Ciais, P., Friedlingstein, P., Peylin, P., Reichstein, M., Luyssaert, S., Margolis, H., Fang, J., Barr, A., … Vesala, T. (2008). Net carbon dioxide losses of northern ecosystems in response to autumn warming. Nature, 451(7174), 49–52.

Pulliainen, J., Aurela, M., Laurila, T., Aalto, T., Takala, M., Salminen, M., Kulmala, M., Barr, A., Heimann, M., … Vesala, T. (2017). Early snowmelt significantly enhances boreal springtime carbon uptake. Proceedings of the National Academy of Sciences, 114(42), 11081–11086.

Quéléver, L. L. J., Kristensen, K., Normann Jensen, L., Rosati, B., Teiwes, R., Daellenbach, K. R., Peräkylä, O., Roldin, P., Bossi, R., … Ehn, M. (2019). Effect of temperature on the formation of highly oxygenated organic molecules (HOMs) from alpha-pinene ozonolysis. Atmospheric Chemistry and Physics, 19(11), 7609–7625.

Rantala, P., Aalto, J., Taipale, R., Ruuskanen, T. M., & Rinne, J. (2015). Annual cycle of volatile organic compound exchange between a boreal pine forest and the atmosphere. Biogeosciences, 12(19), 5753–5770.

Rantala, P., Taipale, R., Aalto, J., Kajos, M. K., Patokoski, J., Ruuskanen, T., & Rinne, J. (2014). Continuous flux measurements of VOCs using PTR-MS – reliability and feasibility of disjunct-eddy-covariance, surface-layer-gradient, and surfacelayer-profile methods. Boreal Environ. Res., 19B, 87–107.

Richardson, A. D., Andy Black, T., Ciais, P., Delbart, N., Friedl, M. A., Gobron, N., Hollinger, D. Y., Kutsch, W. L., Longdoz, B., Luyssaert, S. *et al.* (2010). Influence of spring and autumn phenological transitions on forest ecosystem productivity. Philosophical Transactions of the Royal Society B: Biological Sciences, 365(1555), 3227–3246.

Ruosteenoja, K., Markkanen, T., Venäläinen, Räisänen, P., & Peltola, H. (2018). Seasonal soil moisture and drought occurrence in europe in cmip5 projections for the 21st century. Climate Dynamics, 50, 1177–1192.

Ruuskanen, T., Reissell, A., Keronen, P., Aalto, P. P., Laakso, L., Grönholm, Hari, P., & Kulmala, M. (2003). Atmospheric trace gas and aerosol particle concentration measurements in eastern lapland, finland 1992–2001. Boreal environment research, 8, 335–349.

Schulze, B. C., Wallace, H. W., Flynn, J. H., Lefer, B. L., Erickson, M. H., Jobson, B. T., Dusanter, S., Griffith, S. M., Hansen, R. F., … Griffin, R. J. (2017). Differences in

BVOC oxidation and SOA formation above and below the forest canopy. Atmos. Chem. Phys., 17, 1805–1828.

Sinclair, V. A., Ritvanen, J., Urbancic, G., Statnaia, I., Batrak, Y., Moisseev, D., & Kurppa, M. (2021). Boundary-layer height and surface stability at smear ii, hyytiälä, finland in era5 and observations. Atmospheric Measurement Techniques Discussions, 2021, 1–42.

Sipilä, M., Berndt, T., Petäjä, T., Brus, D., Vanhanen, J., Stratmann, F., Patokoski, J., Mauldin, R. L., Hyvärinen, A.-P., … Kulmala, M. (2010). The role of sulfuric acid in atmospheric nucleation. Science, 327(5970), 1243–1246.

Smith, N. E., Kooijmans, L. M. J., Koren, G., van Schaik, E., van der Woude, A. M., Wanders, N., Ramonet, M., Xueref-Remy, I., Siebicke, L., … Peters, W. (2020). Spring enhancement and summer reduction in carbon uptake during the 2018 drought in northwestern Europe. Philosophical Transactions of the Royal Society B: Biological Sciences, 375(1810), 20190509.

Spracklen, D., Bonn, B., & Carslaw, K. (2008). Boreal forests, aerosols and the impacts on clouds and climate. Philosophical Transactions of The Royal Society A Mathematical Physical and Engineering Sciences, 366(1885), 4613–4626.

Stein, A. F., Draxler, R. R., Rolph, G. D., Stunder, B. J. B., Cohen, M. D., F, & Ngan. (2015). NOAA's HYSPLIT Atmospheric Transport and Dispersion Modeling System. Bull. Amer. Meteor. Soc., 96, 2059–2077.

Stone, D., Whalley, L. K., & Heard, D. E. (2012). Tropospheric oh and ho2 radicals: Field measurements and model comparisons. Chem. Soc. Rev., 41(19), 6348–6404.

Tagesson, T., Schurgers, G., Horion, S., Ciais, P., Tian, F., Brandt, M., Ahlström, A., Wigneron, J. P., Ardö, J., … Fensholt, R. (2020). Recent divergence in the contributions of tropical and boreal forests to the terrestrial carbon sink. Nature Ecology & Evolution, 4, 202–209.

Taipale, R., Kajos, M. K., Patokoski, J., Rantala, P., Ruuskanen, T. M., & Rinne, J. (2011). Role of de novo biosynthesis in ecosystem scale monoterpene emissions from a boreal Scots pine forest. Biogeosciences, 8(8), 2247–2255.

Taipale, R., Ruuskanen, T. M., Rinne, J., Kajos, M. K., Hakola, H., Pohja, T., & Kulmala, M. (2008). Technical note: Quantitative long-term measurements of VOC concentrations by PTR-MS –measurement, calibration, and volume mixing ratio calculation methods. Atmospheric Chemistry and Physics, 8(22), 6681–6698.

Tarvainen, V., Hakola, H., Hellén, H., Bäck, J., Hari, P., & Kulmala, M. (2005). Temperature and light dependence of the VOC emissions of Scots pine. Atmospheric Chemistry and Physics, 5(4), 989–998.

Tunved, P., Ström, J., Kulmala, M., Kerminen, V. M., Maso, M. D., Svenningson, B., Lunder, C., & Hansson, H. C. (2008). The natural aerosol over northern Europe and its relation to anthropogenic emissions–implications of important climate feedbacks. Tellus, B60, 473–484.

Vanhanen, J., Mikkilä, J., Lehtipalo, K., Sipilä, M., Manninen, H. E., Siivola, E., Petäjä, T., & Kulmala, M. (2011). Particle size magnifier for nano-CN detection. Aerosol Science and Technology, 45(4), 533–542.

Vanhatalo, A., Ghirardo, A., Juurola, E., Schnitzler, J., Zimmer, I., Hellén, H., Hakola, H., & Bäck, J. (2018). Long-term dynamics of monoterpene synthase activities, monoterpene storage pools and emissions in boreal scots pine. Biogeosciences, 15, 5047–5060.

Wang, S., Zhang, Y., Ju, W., Porcar-Castell, A., Ye, S., Zhang, Z., Brümmer, C., Urbaniak, M., Mammarella, I., … Folkert Boersma, K. (2020). Warmer spring alleviated the impacts of 2018 european summer heatwave and drought on vegetation photosynthesis. Agricultural and Forest Meteorology, 295, 108195.

Wiedensohler, A., Chen, Y. F., Nowak, A., Wehner, B., Achtert, P., Berghof, M., Birmili, W., Wu, Z. J., Hu, M., … Pöschl, U. (2009). Rapid aerosol particle growth and increase of cloud condensation nucleus activity by secondary aerosol formation and condensation: A case study for regional air pollution in northeastern China. Journal of Geophysical Research, 114.

Williams, J., Crowley, J., Fischer, H., Harder, H., Martinez, M., Petäjä, T., Rinne, J., Bäck, J., Boy, M., … Lelieveld, J. (2011). The summertime Boreal forest field measurement intensive (HUMPPA-COPEC-2010): An overview of meteorological and chemical influences. Atmospheric Chemistry and Physics, 11, 10599–10618.

Wu, C., Chen, J. M., Black, T. A., Price, D. T., Kurz, W. A., Desai, A. R., Gonsamo, A., Jassal, R. S., Gough, C. M., … Blanken, P. D. (2013). Interannual variability of net ecosystem productivity in forests is explained by carbon flux phenology in autumn. Global Ecology and Biogeography, 22(8), 994–1006.

Yan, C., Nie, W., Äijälä, M., Rissanen, M. P., Canagaratna, M. R., Massoli, P., Junninen, H., Jokinen, T., Sarnela, N., … Ehn, M. (2016). Source characterization of highly oxidized multifunctional compounds in a boreal forest environment using positive matrix factorization. Atmospheric Chemistry and Physics, 16(19), 12715–12731.

Yli-Juuti, T., Mielonen, T., Heikkinen, L., Arola, A., Ehn, M., Isokääntä, S., Keskinen, H.-M., Kulmala, M., Laakso, A., … Virtanen, A. (2021). Significance of the organic aerosol driven climate feedback in the boreal area. Nature Communications, 12(15637).

Yu, F., & Luo, G. (2009). Simulation of particle size distribution with a global aerosol model: Contribution of nucleation to aerosol and ccn number concentrations. Atmospheric Chemistry and Physics, 9(20), 7691–7710.

Zeidler, J., & Lichtenthaler, H. K. (2001). Biosynthesis of 2-methyl-3-buten-2-ol emitted from needles of Pinus ponderosa via the non-mevalonate DOXP/MEP pathway of isoprenoid formation. Planta, 213(2), 323–326.

Zha, Q., Yan, C., Junninen, H., Riva, M., Sarnela, N., Aalto, J., Quéléver, L., Schallhart, S., Dada, L., … Ehn, M. (2018). Vertical characterization of highly oxygenated molecules (HOMs) below and above a boreal forest canopy. Atmospheric Chemistry and Physics, 18(23), 17437–17450.

Zikova, N., & Zdimal, V. (2016). Precipitation scavenging of aerosol particles at a rural site in the czech republic. Tellus B: Chemical and Physical Meteorology, 68(1), 27343.